Title: Smooth muscle expression of RNA editing enzyme *ADAR1* controls vascular integrity and progression of atherosclerosis

Authors: Chad S. Weldy[1,2,3], Qin Li[4], João P. Monteiro[1], Hongchao Guo[5], Drew Galls[6], Wenduo Gu[1], Paul P. Cheng[1,3], Markus Ramste[1], Daniel Li[1], Brian T. Palmisano[1], Disha Sharma[1], Matthew D. Worssam[1], Quanyi Zhao[1], Amruta Bhate[6], Ramendra K. Kundu[1], Trieu Nguyen[1], Jin Billy Li[3,6,†], Thomas Quertermous[1,3,6,†,*]

Affiliations:

[1]Department of Medicine, Division of Cardiovascular Medicine, Stanford University

[2]Stanford Center for Inherited Cardiovascular Disease, Stanford University

[3]Stanford Cardiovascular Institute

[4]Department of Genetics, University of Pennsylvania

[5]University of Utah, Cardiovascular Research and Training Institute

[6]Department of Genetics, Stanford University

[†]Co-senior authorship

*__Corresponding Author__:

Thomas Quertermous, MD

William G. Irwin Professor of Medicine

300 Pasteur Drive, Falk CVRC

Stanford, CA 94305

650-498-5794

tomq1@stanford.edu

One Sentence Summary: Smooth muscle expression of RNA editing enzyme ADAR1 regulates activation of double strand RNA sensor MDA5 in novel mechanism of atherosclerosis.

Abstract:

Mapping the genomic architecture of complex disease has been predicated on the understanding that genetic variants influence disease risk through modifying gene expression. However, recent discoveries have revealed that a significant burden of disease heritability in common autoinflammatory disorders and coronary artery disease is mediated through genetic variation modifying post-transcriptional modification of RNA through adenosine-to-inosine (A-to-I) RNA editing. This common RNA modification is catalyzed by ADAR enzymes, where ADAR1 edits specific immunogenic double stranded RNA (dsRNA) to prevent activation of the double strand RNA (dsRNA) sensor MDA5 (*IFIH1*) and stimulation of an interferon stimulated gene (ISG) response. Multiple lines of human genetic data indicate impaired RNA editing and increased dsRNA sensing to be an important mechanism of coronary artery disease (CAD) risk. Here, we provide a crucial link between observations in human genetics and mechanistic cell biology leading to progression of CAD. Through analysis of human atherosclerotic plaque, we implicate the vascular smooth muscle cell (SMC) to have a unique requirement for RNA editing, and that ISG induction occurs in SMC phenotypic modulation, implicating MDA5 activation. Through culture of human coronary artery SMCs, generation of a conditional SMC specific *Adar1* deletion mouse model on a pro-atherosclerosis background, and with incorporation of single cell RNA sequencing cellular profiling, we further show that Adar1 controls SMC phenotypic state, is required to maintain vascular integrity, and controls progression of atherosclerosis and vascular calcification. Through this work, we describe a fundamental mechanism of CAD, where cell type and context specific RNA editing and sensing of dsRNA mediates disease progression, bridging our understanding of human genetics and disease causality.

Main Text:

INTRODUCTION

As coronary artery disease (CAD) is the worldwide leading cause of death (*1*), there is enormous interest to map the genomic mechanisms of disease, establish biological causality, and accelerate therapeutic drug development. Despite the discovery of hundreds of genomic loci associated with CAD (*2-5*) the promise of genome wide association studies (GWAS) to identify new mechanisms for treatment outside of lipid lowering therapy has not been fulfilled. Quantitative trait loci (QTL) studies mapping gene expression QTLs (eQTLs) have helped bridge GWAS variants to their molecular mechanisms (*6, 7*). However, post-transcriptional processes, such as RNA editing, have critical functions in health and disease and genetic determinants of RNA modification are important and poorly appreciated disease mechanisms (*8-10*). Catalyzed by adenosine deaminase acting on RNA enzymes (ADARs), adenosine-to-inosine (A-to-I) RNA editing is a highly frequent RNA modification that is evolutionarily conserved across all metazoan species (*8, 11*). We have recently reported that common genetic variants that modify the frequency of A-to-I RNA editing, loci termed 'editing-QTLs' (edQTL), significantly increase CAD risk as well as numerous other autoinflammatory disorders (*12*). This discovery raises the important possibility that genetically determined RNA editing function is a causal mechanism of CAD, yet the biological underpinning of this relationship is unclear.

Foundational work has revealed that ADAR1 (gene symbol *ADAR*) mediated RNA editing is a novel mechanism of inflammation and disease (*13-16*). A principle function of ADAR1 is to bind double-stranded RNA (dsRNA) in non-coding repetitive elements and convert adenosines to inosines to facilitate the clearance of dsRNA molecules (*17*). This is in contrast to ADAR2 (gene symbol *ADARB1*) that serves to edit coding region of transcripts to modify transcript function (*11*). ADAR1 is ubiquitously expressed across human tissues and its function to edit dsRNA suppresses the sensing of "non-self" dsRNA that is mediated by the cytosolic sensor of dsRNA, MDA5 (gene symbol *IFIH1*) (Fig 1A) (*14, 18, 19*). Mice deficient in Adar1 editing are embryonic lethal due to activation of an interferon-stimulated gene (ISG) response, which is rescued to full life span when Mda5 (*Ifih1*) is also knocked out (*14*). In humans, rare variants

resulting in loss of function in ADAR1 or gain of function in MDA5 result in two severe and clinically overlapping Mendelian interferon mediated disorders, Acardi Goutières Syndrome and Singleton Merton Syndrome, both of which are characterized by a profound early onset vascular calcification phenotype suggesting a link between RNA editing and vascular disease (*20, 21*). This work implicates an 'axis' of ADAR1-dsRNA-MDA5 as a mechanism of inflammatory disease (Fig 1A) and the relationship to CAD is further supported by the notable discovery that rare loss of function variants in MDA5 have been found protective against CAD (*22*).

Here, by analyzing human atherosclerotic plaque single cell RNA sequencing (scRNAseq) data, we identified that vascular smooth muscle cells in atherosclerosis have a uniquely high expression of RNA that require ADAR1 mediated RNA editing to evade MDA5 activation. Through *in vitro* culture of primary human coronary artery smooth muscle cells (HCASMCs) in relevant models, generation of genetic mouse models with conditional deletion of *Adar1* in vascular smooth muscle cells (SMCs) in homozygous loss of function and haploinsufficiency in atherosclerosis, extensive single cell RNA sequencing and histological characterization, we provide crucial data to support the causality behind the genetic determinants of impaired RNA editing and CAD. We identify SMC as a unique mediator of RNA editing and vascular disease and by doing so create a new paradigm linking human genetics, epigenomics, and vascular biology to CAD.

RESULTS

Distinct expression of immunogenic RNA within vascular SMCs in human atherosclerotic plaque

Activation of MDA5 is dependent on the concentration of specific RNA molecules that are prone to the formation dsRNA structures. By combining our data from experimental *in vitro* models (*23*) along with human genetic edQTL analysis (*12*), we generated a putative list of high probability human RNA molecules that are 'immunogenic' and require RNA editing to evade sensing by MDA5. Given the relationship between edQTLs and CAD, we evaluated human scRNAseq data from carotid atherosclerotic plaque (*24*) to determine if there is a cell type specific expression of these immunogenic

RNA. Given that edQTLs that decrease RNA editing increase the risk of CAD, we hypothesized that cells with a higher expression of 'immunogenic' RNAs would be more prone to MDA5 activation if RNA editing was impaired. We evaluated an scRNAseq dataset from human carotid atherosclerotic plaque (*24*) to determine cell clusters and cell types (Fig 1B). We generated a cell module 'score' that summates the expression of all 'immunogenic' RNA and discovered that human SMCs expressed immunogenic RNA at a markedly higher level compared to all other cell types (Fig 1C). This observation suggests a unique role for SMCs in mediating RNA editing within the vessel wall.

SMC phenotypic modulation and ISG induction in atherosclerosis

The formation of atherosclerotic plaque and vascular calcification involves SMCs undergoing a process of epigenetic reprogramming, termed "phenotypic modulation" (25, 26). In this process, SMCs dedifferentiate, down-regulate lineage marker expression, and migrate into the atheroma where these cells then proliferate and differentiate into different progenies that affect the biology of the plaque. Using SMC lineage tracing mouse models of atherosclerosis with single cell RNA and ATAC sequencing of the aortic root, we have previously shown that numerous CAD risk genes mediate disease risk through modification of this phenotypic modulation, including TCF21, ZEB2, AHR, PDGFD and SMAD3 (27-31). Mature SMCs will undergo phenotypic modulation to a more 'fibroblast like' fibromyocyte (FMC) and then into a calcification promoting chondromyocyte (CMC)(29) phenotype in the setting of disease.

We hypothesized that given SMCs express immunogenic RNA at markedly higher levels than other cell types, that insufficient RNA editing and dsRNA sensing, could be identified as expression of key ISGs in the SMC population. To evaluate if there is ISG induction with SMC phenotypic modulation, we performed a subset analysis of the SMC population from a human carotid atherosclerotic plaque dataset (24). Clustering analysis revealed 4 major clusters (cluster '0', '1', '2', and '3') (Fig 1D), where SMCs undergo a process of downregulation of the mature SMC marker MYH11 (Fig 1E) with upregulation of FMC/CMC markers including TNFRSF11B, HAPLN1 and LUM (ex. TNFRSF11B Fig 1F) as SMCs transition from mature SMC cluster '2' to FMC/CMC cluster '0' — a finding we have previously reported (29). However,

findmarker analysis of these clusters identified numerous ISGs as top markers of the FMC/CMC cluster ‘0’, including ISG15, IFI35, IFI16, IFI27, IFIT3 (ex. ISG15, IFI35, IFI16 Fig 1G-I). This finding is suggestive of dsRNA sensing by MDA5 with phenotypic modulation. Top gene ontology (GO) terms of each cluster highlighted clusters ‘2’ and ‘1’ to be defined by ‘smooth muscle contraction’, ‘muscle system process’, and ‘actomyosin structure organization’, while cluster ‘0’ is marked by immune mediated processes including ‘complement activation’ and ‘humoral immune response’ (Fig 1J).

To investigate if ISG induction with SMC phenotypic modulation is conserved in mouse models of atherosclerosis, we evaluated our previously published comprehensive integrated dataset of multiple single cell transcriptomic experiments (32). In this dataset, we evaluated transcriptomic profiles in the aortic root of lineage traced SMCs in hyperlipidemic models of atherosclerosis from multiple publicly available datasets (32). We observed that in comparing between 0 and 16 weeks of high fat diet, SMCs underwent significant phenotypic modulation, marked by downregulation of SMC contractile marker Myh11 (Fig 1K), with upregulation of Col2a1 (Fig 1L), a marker of chondromyocyte formation. With this phenotypic transition, we observed significant upregulation of ISGs including Isg15 (Fig 1M) and Ifit3 (Fig 1N) in these phenotypically modified SMCs. These cells lie at the juncture between FMC and CMC formation and expression was absent in mature SMCs prior to phenotypic modulation.

These data indicate that in atherosclerosis, SMCs uniquely express immunogenic RNA at high levels, and that ISG induction occurs within SMCs undergoing phenotypic modulation — a mechanism that is conserved between mouse and human atherosclerotic disease.

ADAR1 controls global RNA editing and ISG response in human coronary artery smooth muscle cells

To investigate ADAR1 in human SMCs, we used an *in vitro* model of phenotypic modulation with primary human coronary artery smooth muscle cells (HCASMCs) and knocked down (KD) *ADAR* (ADAR1) and *IFIH1* (MDA5) with siRNA transfection paired with bulk RNA sequencing (RNAseq). In this model (Fig 2A), we cultured HCASMCs to confluency, treated with siRNA for 48 hours, and then transitioned to serum free

medium (serum starvation) to induce a mature SMC phenotype marked by high expression of SMC markers (*e.g. ACTA2*, *CNN1*). Following 48 hours of serum starvation, cells were stimulated with either serum replete medium or maintained in a serum free medium for 48 hours. With serum stimulation, HCASMCs subsequently downregulated expression of mature SMC markers, a phenotype akin to phenotypic modulation in the SMC to FMC transition in atherosclerosis (*29*).

With RNAseq data we inferred total RNA editing by detection of G base sequences at RNA editing sites as we have done previously (*12, 33*) (Fig 2B). We observed a notably strong linear relationship between *ADAR* expression and global RNA editing frequency (r^2=0.9509, $p<0.0001$) (Fig 2B&C). Intriguingly, RNA editing frequency significantly decreased with serum stimulation alone (Fig 2C).

ADAR siRNA transfection in serum starved conditions induced a significant gene expression response with 6,351 differentially expressed genes (*FDR <0.05*) (Fig 2D). Top upregulated genes were interferon stimulated genes (ISGs) including *ISG15, IFI6*, *IFI44L*, *IFIT2*, and *IFIT1* (Fig 2D). Importantly, classical interferon genes interferon α, β, and γ (i.e. *IFNA1*, *IFNB1, IFNG*) were either not expressed (*IFNA1* & *IFNG*), or minimally affected by *ADAR* KD in an MDA5 dependent mechanism (*IFNB1*) (Fig S1A-C) with similar minimal effect on the key IFN receptor, *IFNAR1* (Fig S1D).

Top KEGG pathways of upregulated genes indicated a global viral sensing and inflammatory response, including “TNF signaling pathway”, “Influenza A”, “NOD-like receptor pathway”, and “EBV infection”, as well as “Lipid and atherosclerosis” (Fig S1E). GO biological processes similarly revealed “Defense Response to Virus” as the top process (Fig S1F). Downregulated pathways highlighted “Ribosome”, “Focal Adhesion”, and “ECM-receptor interaction” (Fig S1G) and GO terms suggested downregulation of RNA and protein processing with “Cytoplasmic translation” and related terms (Fig S1H). With transfection of both *ADAR* (ADAR1) and *IFIH1* (MDA5) siRNAs we observed that co-KD of *IFIH1* blocked the majority of the gene expression response (Fig 2E).

With serum stimulation (representing phenotypic modulation) we observed *ADAR* KD induced a much greater effect than seen with serum starvation with 12,747 differentially expressed genes (*FDR <0.05*) (Fig 2F). This effect was characterized with a dominant ISG response and appeared nearly entirely dependent on activation of

MDA5 (Fig 2G). When using principal component analysis (PCA) of bulk RNAseq data for each treatment group, we observed that the two dominant principal components tracked with MDA5 activation (PC1) and serum stimulation (PC2), where serum starved cells with *ADAR* KD produced an outwards shift on PC1, and then returned to near baseline with co-KD of *IFIH1* (Fig 2H). With serum stimulation, there was an upwards shift on PC2, and an even greater shift on PC1 with *ADAR* KD, and a return to baseline with co-KD of *IFIH1* (Fig 2I). These findings highlight that the dominant effect of impaired RNA editing in HCASMCs is driven by activation of MDA5 and SMC cell state.

ADAR1 regulates SMC maturation and key CAD transcription factors in phenotypic transition

In this HCASMC model of phenotypic transition, we observed that serum stimulation downregulated mature SMC markers including *ACTA2* and *CNN1* (Fig 2I&J). However, we also observed that *ADAR* KD alone downregulated these SMC markers, an effect that was accentuated with serum stimulation (Fig 2I&J). Using *ISG15* expression as a marker of ISG activation, *ADAR* KD induced an increase in *ISG15* expression (2K), an effect that was enhanced with serum stimulation and entirely blocked with co-KD of *IFIH1* (MDA5) (2K). Interestingly, numerous other key transcription factors with known functions in SMC maturation and risk of CAD (*i.e. KLF4*, *EGR1*, and *ATF3*)(*34*) were similarly affected with *ADAR* KD (Fig 2L-2M).

Global RNA editing is decreased in HCASMC following phenotypic modulation in vitro

In the evaluation of global RNA editing frequency in HCASMC with phenotypic modulation (serum stimulation) with control, *ADAR,* or *ADAR* + *IFIH1* KD, we observed that serum stimulation alone appeared to decrease total RNA editing (Fig 2C). Given we see serum stimulation to increase MDA5 activation with *ADAR* KD, this suggests a potential interaction between phenotypic modulation, decreased RNA editing, and dsRNA formation. To better understand this relationship, we performed a genome wide RNA editing site specific comparison in serum starved and serum stimulated HCASMC (Fig S2). In comparing the mean RNA editing level for each RNA editing site in control

siRNA treated cells in serum starved and serum stimulated conditions, we observed a significant shift where serum stimulated cells have an overall decrease in RNA editing (Fig S2A). Although no specific RNA editing site met genome wide level significance, there was a significant overall net effect to decrease RNA editing across hundreds of RNA editing sites. To then evaluate the effect of *ADAR* KD we performed this editing site specific analysis in the *ADAR* KD with concurrent *IFIH1* KD (minimize the effect of MDA5 activation on ADAR1 editing) that revealed a massive reduction in RNA editing with *ADAR* KD in both serum starved and serum stimulated conditions (Fig S2B&C). From this analysis, we then identified 1,101 differentially edited sites (DES) across 219 genes (Fig S2D&E) that are ADAR1 dependent. The majority of these DES are shared between serum starved and serum stimulated conditions (Fig S2D&E), however we identified 226 sites within 38 genes that are distinct to serum stimulated conditions, and 357 sites within 49 genes that are distinct to serum starved conditions. Evaluation of these genes show no consistent biological pattern where gene ontology enrichment analysis shows no significant pathways (data not shown), however several genes (*TCTA, FN1, GGCX*) have been identified to reside at loci that meet genome wide level significance for CAD (*5*). These data may implicate specific genes that may be responsible for this enhanced MDA5 activation seen with serum stimulation.

TGFβ upregulates ADAR1 and blunts MDA5 activation in HCASMC

As we observed *ADAR* and *IFIH1* (MDA5) to have distinct effects on HCASMC response to serum stimulation (a “synthetic” response), we aimed to further understand how *ADAR* may regulate alternative SMC programming and investigated how *ADAR* and *IFIH1* may regulate HCASMC response to TGF*β* as a ‘contractile’ response. We cultured HCASMC to confluency, treated with siRNA for 48 hours, and transitioned cells to a serum free condition for 48 hours. We then stimulated cells with TGF*β* (10ng/mL) or control for 72 hours before we isolated RNA and performed quantitative PCR. In comparing the effect of serum stimulation or TGF*β* treatment on *ADAR* expression, we observed that serum stimulation induced a small increase in *ADAR* expression (~1.2 fold), however, TGF*β* treatment produced a greater than 2-fold upregulation of *ADAR* (Fig S3A&B). At this timepoint, 7 days after siRNA treatment, *ADAR* expression in the

ADAR KD treatment was found to have normalized in a manner dependent on *IFIH1* (MDA5), indicating that MDA5 activation is stimulating a compensatory upregulation of *ADAR* (Fig S3B). However, when evaluating expression of key ISGs such as *ISG15*, we observed that TGFβ treatment significantly blunted the effect of *ADAR* KD, where a 25-fold upregulation of *ISG15* with *ADAR* KD in serum starved conditions was limited to less than 10-fold upregulation with TGFβ treatment (Fig S3C). In our serum stimulation study, *ADAR* KD induced a marked upregulation of *IFIH1* (MDA5) that was exacerbated with serum stimulation in a pattern that was consistent with all other ISGs (Fig S3D). However, TGFβ treatment markedly reduced this effect of *ADAR* KD (Fig S3E). We further evaluated expression of *PKR*, a key ISG that acts to control cellular signaling following MDA5 activation (*35*). Here, we found *PKR* to similarly be upregulated by *ADAR* KD, however this effect is significantly reduced with TGFβ treatment (Fig S3F). This finding suggests that TGFβ treatment regulates expression of *ADAR* and perhaps implicates a mechanism of TGFβ to control dsRNA editing by ADAR1 and dsRNA sensing by MDA5.

Loss of ADAR1 regulates the transcriptomic and inflammatory response to calcification in vitro

To model SMC calcification *in vitro*, we cultured an immortalized HCASMC line under high calcium/phosphate culture conditions as has been previously reported (*36*). In this model, SMCs begin to form deposits that stain with Alizarin red, consistent with calcium crystals and has been proposed to represent vascular calcification (*36*). Following siRNA transfection for 48 hours, we cultured cells for 7 days with pro-calcification medium under low serum (1%) conditions and performed bulk RNAseq. After 7 days, calcification deposits became visible, however with *ADAR* KD, there was a significant phenotypic change with increased cell death and increased density of calcium deposits — an effect that was blocked with co-KD of *IFIH1* (Fig S4A&B). Calcification medium under scramble siRNA treatment promoted a significant gene expression response with 584 differentially expressed genes (*FDR <0.05*) (Fig S3C). Top upregulated genes include numerous BMP related signaling genes including *FBLN5*, *FMOD*, and

RANBP3L (Fig S4D-F), effects that have been previously reported (*36*). However, with *ADAR* KD this effect was blunted in an MDA5 dependent mechanism (Fig S4D-F).

Calcification did not overtly activate MDA5 as measured by expression of *ISG15* (Fig S4G&H), however, *ADAR* KD modified the HCASMC inflammatory response to calcification. Calcification had minimal effect on expression of NFκB (*NFKB1*), however with *ADAR* KD *NFKB1* is modestly upregulated and is further upregulated with calcification in *ADAR* KD cells, an effect blocked with co-KD of *IFIH1* (Fig S4I). This observation revealed a unique relationship where calcification induced a distinct proinflammatory effect only with concurrent *ADAR* KD and MDA5 activation. Similar effects were observed for numerous proinflammatory signaling and matrix proteins including *JUND*, *MMP1*, and *MMP10* (Fig S4J-L).

SMC specific Adar1 maintains vascular integrity and survival in vivo

Although prior reports have implicated SMC specific RNA editing in mediating phenotypic response (*37, 38*), the relationship between deficient SMC RNA editing, MDA5 activation, vascular inflammation, and atherosclerosis has not been investigated. Here, we bred a mouse model with four distinct alleles, including *Adar1*$^{fl/fl}$ (exon 7-9), a tamoxifen inducible SMC specific Cre-recombinase (*Myh11*^{CreERT2}), a lineage tracing fluorophore (*ROSA*^{tdTomato}), on a hyperlipidemic pro-atherosclerosis genetic background (*ApoE*$^{-/-}$) (Fig 3A). A total of 56 mice were treated, comparing *SMC-Adar1*$^{-/-}$, *SMC-Adar1*$^{-/+}$ (*Adar1*$^{fl/WT}$, *Myh11*^{CreERT2}, *ROSA*^{tdTomato}, *ApoE*$^{-/-}$), and control (*Adar1*$^{WT/WT}$, *Myh11*^{CreERT2}, *ROSA*^{tdTomato}, *ApoE*$^{-/-}$) genotypes. We observed that at day 4, *SMC-Adar1*$^{-/-}$ mice became notably ill as characterized by weight loss, piloerection, and a hunched posture, a phenotype that was not present in *SMC-Adar1*$^{-/+}$ or control genotype animals. We observed mortality in the *SMC-Adar1*$^{-/-}$ mice at this time and by 14 days, 10/20 (50%) mice had died (Fig 3B). Gross dissection and visual inspection of *SMC-Adar1*$^{-/-}$ mice did not reveal any notable findings of the lungs, heart, or intestines however visual appearance of the aorta suggested petechial hemorrhage and erythema (Fig 3C). H&E staining (Fig 3D&E), fluorescent imaging (Fig 3F&G), bright field imaging (Fig 3H), Cd68 immunostaining (Fig 3I), and Masson's trichrome staining (Fig 3J) of ascending and descending aortic tissue in 6 *SMC-Adar1*$^{-/-}$ mice revealed a loss of

elastin organization (present in 6/6 mice), dissociation of the matrix at the adventitial aspect with associated 'ballooning' out and separation of layers (present in 3/6 mice), with evidence of intramural hemorrhage (present in 2/6 mice) (Fig 3D-H, Fig S5). These sites of ballooning occurred with complete loss of tdTomato SMCs at the adventitial aspect (Fig 3F&G). H&E staining of the aorta confirmed severe loss of organization of the elastin matrix and evidence of intravascular hemorrhage with further discovery of dense cellular infiltrate into the adventitia (Fig 3D&E). These patterns were not observed in control mice (Fig 3E). Immunostaining for CD68 revealed macrophage cell infiltration from the luminal as well as the adventitial aspect of the vessel wall (Fig 3I). Additional Masson's trichrome stain to evaluate for fibrosis revealed evidence of intra-medial collagen deposition (Fig 3J).

In this model, there was a rapid and early inflammatory response that resulted in profound weight loss and mortality. Although the cause of death was not immediately apparent, as gross examination and H&E sections of liver, lung, and heart were nonrevealing, the acute systemic inflammatory response is likely eliciting death through a multifactorial mechanism akin to a systemic inflammatory response. There was no evidence of aortic rupture as a cause of death. However, mice that survived this period remained underweight and ill in appearance until ~7 months of age. Importantly, no mice that were taken past this 2-week timepoint regained weight or lived a normal lifespan. Dissection of mice at this 7-month timepoint demonstrated dense fecal impaction of the large intestine, consistent with bowel obstruction, a finding not seen at earlier timepoints.

Single cell RNA sequencing reveals SMC Adar1 controls ISG activation, phenotypic response, and macrophage infiltration into the vessel wall

To further characterize the vascular response of SMC specific *Adar1* KO in mouse, we performed single cell RNA sequencing (scRNAseq) of the aortic root and ascending aorta of *SMC-Adar1*$^{-/-}$ mice at day 14 following tamoxifen dosing. With a total of 10 individual scRNAseq captures, we characterized over 50,000 cells with high sequencing depth (>50K reads per cell). Using dimensionality reduction with UMAP as we have done previously (*39, 40*), we observed *SMC-Adar1*$^{-/-}$ aortic cells to have a dramatic

transcriptomic change in comparison to control genotype (Fig 4A). Cluster analysis identified 13 main clusters, including 3 SMC clusters — a control SMC cluster marked by mature contractile markers (i.e. *Myh11* and *Cnn1*), and two SMC clusters that represented cells with distinct transcriptomic signatures secondary to SMC *Adar1* KO that are marked by tdTomato (clusters SMC_cAdar1_KD1; SMC_cAdar1_KD2) (Fig 4B&C). Genes expressed by cells in these two clusters were found to show gene ontology (GO) enrichment for terms related to 'response to interferon beta', 'response to virus', 'defense response to virus' as top GO terms (Fig S6). Using *Isg15* as a marker of MDA5 activation, clusters SMC_cAdar1_KD1 and SMC_cAdar1_KD2 were marked by notably high expression of *Isg15* (Fig 4D). To validate this finding and characterize the location of *Isg15* expression, we performed RNAscope on aortic tissue from *SMC-Adar1*$^{-/-}$ mice. We observed robust *Isg15* expression within the vessel wall that was highest at the luminal aspect of the media, with additional expression within the adventitia (Fig 4E).

Within tdTomato lineage traced SMCs, conditional *Adar1* KO produced marked gene expression changes with 2,382 differentially expressed genes (*FDR<0.05, log2FC>0.1*), with notable increase in ISGs. In comparing clusters SMC_cAdar1_KD1 and SMC_cAdar1_KD2, SMC_cAdar1_KD2 was marked by higher expression of numerous inflammatory signaling genes (i.e. *Isg15*, *Ccl5*, *Cxcl10*) (Fig S7A).

Importantly, consistent with our *in vitro* findings (Fig S1A-D), there was only modest activation of classical interferon genes with no observed expression of *Ifna1* and minor activation of *Ifnb1* (Fig 4F). Similarly, we observed minimal expression of IL6 family cytokines (i.e. *Il6*) with *SMC-Adar1*$^{-/-}$ (Fig S7B). The minimal expression of these markers appeared limited to the more proinflammatory SMC_cAdar1_KD2 cluster. In addition, consistent with our *in vitro* findings, we observed that SMC *Adar1* KO led to downregulation of mature SMC markers (Fig S7C). By comparing the three major SMC clusters, expression of *Cnn1* and *Myh11* decreased in a pattern consistent with increasing MDA5 activation (Fig S7C).

There was a new distinct fibroblast population seen only with SMC *Adar1*$^{-/-}$ and is marked by ISGs and high expression of *Ly6a* (Sca1) (Fig 4B, Fig S7D), consistent with a proinflammatory adventitial fibroblast population (*41*). Similarly, in SMC *Adar1*$^{-/-}$ there

was a loss of cells within the ‘Fibro_1’ cluster that was only seen in controls (Fig 4B), suggesting a dynamic shift in gene expression from resident fibroblasts to this new reparative and inflammatory cell cluster. In addition, there was a large infiltrating macrophage population marked by high *Cd68* (resident macrophage cluster – ‘Mac’, infiltrating macrophage cluster – ‘Mac_2’) (Fig 4B, Fig S7E) with an additional small T cell population with SMC *Adar1*$^{-/-}$ marked by high *Gzma*, *Cd3g*, and *Cd52*, suggestive of a cytotoxic T lymphocyte (CTL) population (Fig 4B, Fig S7F). These data indicate that with loss of *Adar1* within SMCs, a profound vascular response occurs throughout the vessel wall that is coordinated by SMCs.

Receptor-ligand interaction modeling implicates CCL5:CCR5 to coordinate macrophage infiltration in SMC-Adar1$^{-/-}$ mice

To better understand the cell-cell communications that mediate this response, we performed an inference analysis of cell-cell communication focused on receptor-ligand interactions (CellChat) (*42*). This analysis revealed that with SMC *Adar1*$^{-/-}$, SMC clusters SMC_cAdar1_KD1 and SMC_cAdar1_KD2 are notably high outward senders of CCL signaling markers (Fig 4G). When interrogating the specific signaling pairs, Ccl5:Ccr5 was the dominant interaction (Fig 4H). A circos plot depicting Ccl5:Ccr5 interaction strength revealed dominant outward interaction arising from SMC_cAdar1_KD1 and SMC_cAdar1_KD2 clusters with key receiving clusters being resident macrophage, infiltrating macrophage, and T cell populations (Fig 4I). Feature plots of Ccl5 and Ccr5 further revealed the distinct expression of Ccl5 within SMCs following *Adar1* KD and Ccr5 within macrophage populations (Fig 4J&K). Evaluation of the next top 3 interaction pairs (Ccl2:Ccr2; Ccl4:Ccr5, Ccl7:Ccr2) suggested that following Ccl5:Ccr5 interaction, Ccl2 and Ccl7 arising from SMC_cAdar1_KD2, Fibro_Sca1_hi, and macrophage cell populations appeared to interact with Ccr2 within macrophage and T lymphocyte populations (Fig S7G-L). These data suggested that Ccl4 from resident and infiltrating macrophage clusters further signaled through Ccr5 on these same cell clusters (Fig S7J&K). Activation of CCR5 has been previously identified as a key regulator of antiapoptotic signaling in macrophage cells in response to viral infection (*43*). Our

observation provides a unique insight that following the loss of SMC *Adar1*, Ccl5:Ccr5 acts as a dominant regulator of macrophage infiltration and macrophage cell survival.

Haploinsufficiency of MDA5 is sufficient to protect against SMC Adar1$^{-/-}$ mice

Our *in vitro* work indicates MDA5 to be the principal mediator of downstream signaling with ADAR1 KD in SMC, however it remains unclear if this relationship is true *in vivo*. In addition, it is unclear if only partial inhibition of MDA5 can prevent overt ISG activation, a model more akin to what might be achieved with future pharmacologic inhibition. To test this, we bred the SMC *Adar1* KO mouse onto a constitutive KO of *Ifih1* (Mda5) on both a heterozygous and homozygous background generating mice that are *SMC-Adar1$^{-/-}$* + *Mda5$^{-/+}$* (*Adar1$^{fl/fl}$*, *Ifih1$^{-/+}$, Myh11^{CreERT2}*, *ROSAtdTomato*, *ApoE$^{-/-}$*) and *SMC-Adar1$^{-/-}$* + *Mda5$^{-/-}$* (*Adar1$^{fl/fl}$*, *Ifih1$^{-/-}$, Myh11^{CreERT2}*, *ROSAtdTomato*, *ApoE$^{-/-}$*). Following the same model as shown previously (Fig 3), we performed an additional experiment using litter-mate controlled mice with tamoxifen treatment for a total of 32 mice (12 SMC-*Adar1$^{-/-}$*, 8 *SMC-Adar1$^{-/-}$* + *Mda5$^{-/+}$*, and 12 *SMC-Adar1$^{-/-}$* + *Mda5$^{-/-}$*). Mice that were homozygous SMC *Adar1* KO with MDA5 WT had severe weight loss and significant mortality, with 10/12 (83%) *SMC-Adar1$^{-/-}$* mice dying prior to the 14-day timepoint and greater than 30% loss of total body weight by 7 days for the 6 mice that survived to the 7-day timepoint (Fig 5A-C). Both *SMC-Adar1$^{-/-}$* + *Mda5$^{-/+}$* and *SMC-Adar1$^{-/-}$* + *Mda5$^{-/-}$* mice showed minimal weight loss and no mortality, and visually appeared largely unaffected by *Adar1* KO at this 2-week timepoint (Fig 5A-C). *SMC-Adar1$^{-/-}$* + *Mda5$^{-/+}$* mice have been taken out to 24 weeks following tamoxifen dosing and continue to show minimal phenotype, demonstrating that MDA5 is required to initiate this severe phenotype with SMC *Adar1* KO (Fig 5D). Intriguingly, a portion of both *SMC-Adar1$^{-/-}$* + *Mda5$^{-/+}$* and *SMC-Adar1$^{-/-}$* + *Mda5$^{-/-}$* mice (2/8 and 4/12, respectively) did lose significant weight within the first week, however had significant weight recovery by week 2 (Fig 5C). This suggests that although MDA5 deletion protects against mortality and any major phenotype, that alternative dsRNA receptors such as RIG-I may be mediating a partial inflammatory response.

SMC specific haploinsufficiency of Adar1 activates the ISG response in atherosclerosis and increases vascular chondromyoctye formation

Although conditional homozygous deletion of *Adar1* in SMCs caused a profound and rapid onset phenotype *in vivo* in a manner dependent on *Mda5*, we aimed to understand if haploinsufficiency of *Adar1* in SMCs, where mice appear to have no discernable phenotype, may lead to MDA5 activation, SMC phenotypic modulation, and progression of atherosclerosis. To do this, we used the *SMC-Adar1*$^{-/+}$ (*Adar1*$^{fl/WT}$, *Myh11*^{CreERT2}, *ROSAtdTomato*, *ApoE*$^{-/-}$) mice with genotype controls (*Adar1*$^{WT/WT}$, *Myh11*^{CreERT2}, *ROSAtdTomato*, *ApoE*$^{-/-}$), dosed with tamoxifen at 7.5 weeks of age, and placed on high fat diet for 16 weeks (Fig 6A). In this model, mice developed pronounced atherosclerosis as we have shown previously (*28, 29, 39, 40*). *SMC-Adar1*$^{-/+}$ and control mice had no differences in weight or lipid analysis (cholesterol, LDL, HDL, triglycerides) at this 16 week timepoint (Fig S8). To understand the cellular resolution of the vessel wall, at 16 weeks, we performed scRNAseq of the aortic root and ascending aorta. With a total of 12 scRNAseq captures analyzing over 70,000 cells comparing *SMC-Adar1*$^{-/+}$ and control genotypes, we observed expected distinct cell clusters of SMCs, fibroblasts, endothelial cells, macrophage cells, and T cells (Fig 6B). Lineage traced SMCs demonstrated distinct SMC clusters as we have previously observed and have been consistent with phenotypic modulation(*29, 39, 40*), with a mature SMC cluster, a fibromyocyte (FMC) cluster, and a calcification promoting chondromyocyte (CMC) cluster of cells (Fig 6B). Importantly, *SMC-Adar1*$^{-/+}$ mice showed a large and distinct new SMC population residing between the mature SMC population and the FMC population (Fig 6B). Characterization of this population by *findmarker* analysis demonstrated this cluster to express numerous markers of ISG activation (i.e. *Ifit3*, *Ifit1*, *Isg15*) consistent with MDA5 activation. Analysis of *Isg15* as a marker of ISG activation revealed notable expression within this SMC cluster, termed ‘SMC_ISG’ (Fig 6B&C).

To focus on the lineage traced SMC population, we performed an analysis on the ‘SMC’, ‘SMC_ISG’, ‘FMC’, and ‘CMC’ clusters. With subsequent dimensionality reduction and repeat clustering, UMAP visualization highlighted the marked effect of SMC *Adar1* haploinsufficiency in SMC phenotypic states in atherosclerosis (Fig 6D&E). Top 10 marker genes and GO term enrichment for ‘SMC’, ‘SMC_ISG’, ‘FMC’, and

‘CMC’ clusters reveals the SMC_ISG cluster to be marked by ISGs including *Ifit3, Isg15, Ifit1,* and *Irf7* and GO terms highlighting “response to virus”, “response to interferon-beta”, and “defense response to virus” (Fig S9A&B). Evaluation of SMC marker *Myh11* demonstrated downregulation of mature contractile markers with phenotypic modulation (Fig S10A) with associated upregulation of FMC and CMC markers (i.e. *Tnfrsf11b*, *Col2a1*, and *Acan*) (Fig S10B-D). Separation by genotype further highlighted that with *SMC-Adar1*$^{-/+}$ mice, there was a shift away from mature SMCs, marked increase in the SMC_ISG cluster, and an increase in CMC (Fig 6E&F). A featureplot of *Isg15* expression in SMC subsets highlighted a possible relationship between the ‘SMC_ISG’ and ‘CMC’ clusters (Fig 6G). Comparison of the expression of CMC markers *Col2a1* and *Acan* between genotypes demonstrated an increase in CMC cells with *SMC-Adar1*$^{-/+}$ mice consistent with this finding (Fig S10E&F). This finding suggests that ISG activation from SMC *Adar1* haploinsufficiency in atherosclerosis may be contributing to CMC formation and vascular calcification.

Lineage trajectory analysis of vascular chondrogenesis reveals a distinct ISG dependent trajectory

To investigate the potential for this SMC lineage relationship, we performed pseudotime inference and cellular trajectory analysis with Slingshot (*44*). By increasing clustering resolution we generated 14 high resolution clusters of all tdTomato lineage traced SMCs and performed Slingshot inference to understand the cellular trajectory between mature SMC to CMC clusters. In this analysis, we observed only 2 distinct trajectories between SMC and CMC (Fig 6H). Importantly, one trajectory excludes all SMC_ISG clusters, while a second is dependent on SMC_ISG clusters (Fig 6H). This suggests two distinct cellular trajectories to CMC formation, with one trajectory dependent on ISG activation, while a second is ISG independent. This observation of an ISG dependent trajectory to CMC formation with increased CMC formation with SMC *Adar1* haploinsufficiency in atherosclerosis implicates a disease context specific activation of MDA5 with inadequate RNA editing and disease progression.

To better understand the top genes driving this ISG dependent trajectory, we performed findmarker analysis on all high-resolution clusters and evaluated the top

markers for each cluster in sequence of the ISG dependent pathway (Fig S11A). This analysis highlights that as SMC lose expression of contractile markers such as *Myh11* and *Acta2*, they begin to express numerous ISGs. Initially, there is high expression of *Irf7*, *Isg15*, *Ifit1*, which is then followed by increasing expression of *Ly6a*, *C3*, *Cxcl12*, and other FMC markers such as *Dcn* and *Tnfrsf11b*, before SMCs have marked expression of key CMC genes such as *Col2a1*, *Chad*, *Fmod*, and *Spp1* (Fig S11A). To further understand the pathways driving this ISG dependent trajectory, we selected the gene markers of the high-resolution clusters that are distinct to the ISG trajectory and performed gene ontology pathway analysis (Fig S11B). Here, we identified top viral immune response pathways including *'Coronavirus Disease'*, *'Influenza A'*, and *'Epstein-Barr Virus infection'*, driven by genes such as *Jun, Ccl2*, *Il6*, *Nfkb1*, and this analysis also reveals key JAK/STAT signaling molecules such as *Stat3* and *Jak1* (Fig S11B). In addition to immune pathways, *'Focal Adhesion'* and *'Regulation of Actin Cytoskeleton'* are highlighted, driven by genes such as *Rock1*, *Itgb1*, *Egfr,* PDGFs, and *Map2k1*, suggesting a distinct interrelationship between activation of JAK/STAT and key immune signaling pathways influencing focal adhesion pathways (Fig S11B).

To determine the location of MDA5 activation within the plaque and vessel wall, we performed RNA scope on aortic root sections for *Isg15*. In control mice, we observed scattered *Isg15* expression within the media, the base of the plaque and extending up to the region beneath the cap, as well as in the adventitia (Fig 6I). However, in *SMC Adar1*$^{-/+}$ mice we observed a marked increase in *Isg15* signal, with intense *Isg15* expression within the media, throughout the plaque, and within the adventitia (Fig 6J). Signal of *Isg15* RNAscope positive area in the vessel wall was quantified (Fig S12A) and location of *Isg15* signal was compared to signal of chondromyocyte marker *Col2a1*, where we reveal that cells that express *Isg15* reside in spatially distinct regions compared to *Col2a1* (Fig S12B-C). These data suggest ISG activation in atherosclerosis in control mice, however this effect is markedly increased with haploinsufficiency of *Adar1* within the vascular SMC.

SMC specific haploinsufficiency in Adar1 increases plaque size and calcification in atherosclerosis

We performed histological analysis of the aortic root for *SMC-Adar1*$^{-/+}$ and control genotype mice after 16 weeks of high fat diet (n=13 each group). Using fluorescent imaging of tdTomato and autofluorescence (elastin), we quantified plaque area and plaque area normalized to total area of the internal elastic lamina area (IEL) (Fig 7A-D). We observed that *SMC-Adar1*$^{-/+}$ mice had a significant increase in plaque area, an effect that remained following normalization to overall area of the IEL (Fig 7A-D). Notably, quantification of the area of the media (area between IEL and external elastic lamina, EEL), we observed *SMC-Adar1*$^{-/+}$ mice to have a significant reduction, an effect that remained following normalization to the total area of the EEL (Fig 7E&F). When plaque area was normalized to media area, the observed effect with *SMC-Adar1*$^{-/+}$ mice was further enhanced (Fig 7G). In addition, we observed total area of the EEL to be increased (Fig 7H), suggesting an increased outward remodeling of the plaque. Given our observation from single cell data that suggested increased chondromyocyte formation, we evaluated the effect of SMC *Adar1* haploinsufficiency on calcification by Ferangi Blue Chromogen staining (Fig 7I-L). We observed *SMC-Adar1*$^{-/+}$ mice to have a significant increase in total Ferangi Blue staining by area (Fig 7K), an effect that remained with normalization to plaque area (Fig 7L). These findings demonstrate that SMC *Adar1* haploinsufficiency accelerate the formation atherosclerotic plaque area and calcification.

SMC specific haploinsufficiency of Adar1 increased SMC lineage traced cell content in plaque without a change in acellular area

Our data suggests that impaired RNA editing in vascular SMC leads to increased plaque area and decreased media thickness, implicating increased SMC migration out of the media and into the plaque. To investigate this, we quantified tdTomato positive area within plaque as a marker of SMC lineage traced cells integrating into the plaque. Here, we observed that in SMC Adar1$^{-/+}$ mice, the percent tdTomato area within plaque is increased compared to control mice (p=0.0024)(Fig S13A-B). To then understand if this increased SMC migration into the plaque results in a similar increase in tdTomato area within the cap of the plaque, we measured the tdTomato area of the top 30μm segment of the cap (Fig S13C). Here, we did not observe a significant difference,

although there was a greater mean tdTomato area in the SMC Adar1$^{-/+}$ mice (p=0.0749).

To evaluate if there is increased acellular area within the plaque, we performed Masson's Trichrome stains on lesions and quantified acellularity by tracing the plaque and subtracting all area that has stain to then be able to quantify all acellular area. Here, when normalizing acellular area by plaque area, we observed no difference between genotypes (Fig S13D-E).

SMC specific haploinsufficiency in Adar1 has minimal effect on macrophage content in atherosclerosis

With a subsetted analysis on all non-tdTomato lineage traced cell populations, we observed that *SMC-Adar1*$^{-/+}$ mice have a small increase in total macrophage cell populations in this 16-week atherosclerosis model (39.7% vs 35.2% of all non-tdTomato cell population) (χ^2 *p=3.66E-26*) with minimal change in cell numbers across all other cell types (Fig 8A&B). As we have shown that CCL signaling and Ccl5:Ccr5 appeared to be the dominant driver of macrophage recruitment in *SMC-Adar1*$^{-/-}$ mice, we investigated if these signaling molecules were similarly upregulated in this 16-week *SMC-Adar1*$^{-/+}$ atherosclerosis model. When performing receptor-ligand interaction analysis using CellChat (*42*), we observed the 'SMC_ISG' cluster to have absent CCL signaling and did not appear to act as a sender, receiver, mediator, or influencer (Fig 8C&D). We then performed Cd68 immunohistochemical staining on aortic root sections to evaluate for Cd68 positive area within the plaque between control and *SMC-Adar1*$^{-/+}$ mice (Fig 8E-I). We observed that the total Cd68 positive area within the plaque was significantly greater in the *SMC-Adar1*$^{-/+}$ mice (Fig 8G), however this effect only trended towards significance when normalized to plaque area (Fig 8H) or area of the total vessel at the internal elastic lamina (Fig 8I). The lack of a major effect on macrophage content at this timepoint for this 16-week atherosclerosis *Adar1* haploinsufficiency model is in contrast to our 2-week SMC-*Adar1* KO model (Fig 3) and likely reflects a 'dose-dependent' response of SMC *Adar1* gene deletion, MDA5 activation, and *Ccl5* expression.

DISCUSSION

Both academic and industry leaders are leveraging the power of human genetics to drive discovery in the goal to define causal disease biology (*45*). The rapid pace of identifying novel genomic loci that meet genome wide level significance for complex disease has resulted in notable challenges of target prioritization within a locus (*46*), as well as prioritization for therapeutic drug development (*47*). However, the association of edQTL and CAD risk, where impaired RNA editing increases CAD risk, implicates a common disease pathway that is largely dependent on one gene product. Strikingly, 20% of CAD risk loci examined colocalized with edQTL loci (*12*). With a new understanding of the genetic determinants of RNA editing and dsRNA sensing as an underlying etiology of coronary artery disease and other inflammatory disorders (*12*), there is a significant need to define how this mechanism influences disease risk.

Here, we provide a crucial link between the human genetics that implicate RNA editing and dsRNA sensing in atherosclerosis and the biological underpinnings of this disease association. We reveal a unique aspect of biology, where the vascular SMC has a distinct requirement for ADAR1 mediated RNA editing to evade dsRNA sensing by MDA5. Analysis of human atherosclerotic plaque scRNAseq data indicate a unique pattern where SMCs express immunogenic RNA at high levels and that ISG activation — suggestive of MDA5 activation with inadequate RNA editing — occurs with SMC phenotypic modulation in both human and mouse data. We further show that deletion of SMC specific *Adar1* in adult mice results in loss of vascular integrity and significant mortality (Fig 3) where scRNAseq analysis of aortic tissue reveals distinct ISG activation and a complex transcriptional response and inflammatory cell recruitment within the vessel wall (Fig 4). This highlights the absolute requirement for *Adar1* within the vascular SMC. Importantly, in 16-week atherosclerosis studies in *Adar1* haploinsufficient mice, scRNAseq reveals ISG activation in SMCs in a cell type and context specific mechanism driving phenotypic modulation, vascular chondromyocyte formation, and to a lesser extent macrophage recruitment (Fig 6), and that this coincides with increased plaque area, decreased thickness of the media, and increased calcification (Fig 7). This indicates that SMC *Adar1* haploinsufficiency facilitates thinning of the media while increasing plaque area, suggesting increased SMC migration into the

plaque. In addition, we reveal that the severe phenotype of homozygous deletion of *Adar1* in SMC *in vivo* can be prevented with deletion of MDA5, where even haploinsufficiency of MDA5 eliminates the mortality phenotype (Fig 5), providing crucial insight into the potential for therapeutically targeting MDA5.

These findings highlight an important new concept, that the need for RNA editing to evade MDA5 activation not only occurs in a cell type specific manner, but a cellular context specific manner. Two prior studies have investigated the role of SMC *Adar1* in haploinsufficiency in SMC phenotypic modulation, focused on carotid injury (*38*) and an angiotensin II model of abdominal aortic aneurysm (AAA) (*37*). In these reports, the authors reported that loss of SMC Adar1 prevented phenotypic modulation, however no investigation into potential MDA5 activation was performed. Our data reported here appears in contrast to this finding, however our findings implicate that the effect of loss of ADAR1 on phenotypic transition is dependent on MDA5 activation and occurs in a 'dose dependent' mechanism where increasing MDA5 activation has a greater effect. The SMC *Adar1*$^{-/+}$ model is unique in that in haploinsufficiency there is no immediate activation of MDA5, however in specific cellular contexts immunogenic RNA formation appears to 'max out' the RNA editing capacity of the single *Adar1* allele leading to MDA5 activation. This effect is overt in a 16-week high fat diet model of atherosclerosis, however this was perhaps not evident in either of the prior short term carotid injury or AAA models. However, a recent discovery that MDA5 (*IFIH1*) is a key locus in a large GWAS of AAA raises an intriguing hypothesis that ADAR1 and MDA5 are causal mechanisms in AAA formation (*48*).

Our data indicate that SMC phenotypic modulation is a cellular context that requires heightened RNA editing and that deficient RNA editing with SMC *Adar1* heterozygous mice leads to MDA5 activation that accelerates SMC phenotypic changes and disease state. These data reveal distinct trajectories to SMC formation of the vascular chondromyocyte (CMC), where ISG activation through MDA5 facilitates the formation of CMCs and vascular calcification. This effect of MDA5 activation on SMC phenotypic state is consistent with prior work investigating the role of ADAR1 and MDA5 on cellular proliferation and cell death (*13*). ADAR1, through its role of editing dsRNA and preventing MDA5 activation, is crucial in regulating proliferation and deterring

endogenous dsRNA from triggering transcriptional shutdown and apoptotic cell death through activation of PKR (*EIF2AK2*) (*13*). Intriguingly, in this report, with initial KD of *ADAR1*, cell proliferation was found to be increased, however with mounting MDA5 activation there was ultimately PKR activation and transcriptional shut down and cell death (*13*). This effect, where initial loss of ADAR1 stimulates proliferation and cell state transitions, is perhaps consistent with modifying a cell state similar to SMC to FMC transition in atherosclerosis in our SMC *Adar1*$^{-/+}$ model. However, with overwhelming MDA5 activation as seen in our SMC *Adar1*$^{-/-}$ model, there is transcriptional shut down, cell death, and major vascular effect.

Importantly, although classical inflammatory mechanisms have been implicated in the pathogenesis of atherosclerosis and tremendous interest has been placed in the potential to inhibit these pathways to treat disease (*49*), only a small minority of GWAS loci in CAD implicate inflammatory pathways (*2-5*). This finding raises the question as to the overall weight of effect for disease causality for such inflammatory mediators (i.e. IL6, TNFα, and IL1β). The relatively minimal benefit of IL1β antagonism in CAD (*50*) may suggest an overall limited potential to treat disease through inhibition of these inflammatory mediators. However, dsRNA sensing by MDA5 and ISG activation as an overarching mechanism provides a new avenue of understanding as to how inflammatory mechanisms are driving disease biology. Our data demonstrates that ISG activation occurs in SMCs during atherogenesis, however the exact function of these ISGs remains unclear. The function of ISGs has been previously reviewed (*51*), however, ultimately IFN and ISGs serve key roles to regulate cellular viral immune response, likely through driving transcriptional shutdown in a PKR dependent mechanism of cells infected by a viral pathogen. Importantly, Type I interferon induces JAK/STAT intracellular signaling pathways (*51*), a finding we observed in our ISG dependent cellular trajectory in SMC phenotypic transition (Fig 6H & Fig S11). This finding perhaps suggests that JAK/STAT is an important regulator of this trajectory. Specific ISGs have distinct roles in fighting viral infection, for example on inhibiting viral entry (IFITM1/2/3), mRNA synthesis (IFI16), protein synthesis (PKR), and mRNA degradation (ISG20) (*51*). The mechanism by which specific ISGs may modify atherosclerosis within the vessel wall remains unclear. However, an important

observation from human genetics is that edQTL loci, which ultimately implicates dsRNA formation, MDA5 activation, and ISG induction, to be a greater driver of disease heritability than all eQTLs in CAD (*12*). This data presented here further implicates a specific mechanism of disease while highlighting a unique opportunity to leverage this biology for therapeutic development by prioritizing the inhibition of dsRNA sensing and downstream activation of MDA5.

MATERIALS AND METHODS

Data availability

All raw and processed sequencing data are deposited in the National Center for Biotechnology Information Gene Expression Omnibus. Bulk and single cell RNA sequencing data is available through accession IDs GSE254862 and GSE255661 respectively.

Mouse Models

To generate SMC-specific deletion of Adar we used the *Adar*$^{flox/flox}$ allele (exon 7-9 floxed; MGI allele: Adar$^{tm1.1Phs}$; MGI:3828307) as we have reported previously(*52*), crossed onto the validated SMC-specific mouse Cre allele (Myh11^{CreERT2}) combined with the floxed tandem dimer tomato (tdT) fluorescent reporter protein gene knocked into the ROSA26 locus (B6.Cg-Gt(ROSA)26Sortm14(CAGtdTomato)Hze/J) and ApoE$^{-/-}$ alleles (Adar$^{flox/flox}$, Myh11^{CreERT2}, ROSAtdT/+, ApoE$^{-/-}$). To induce homozygous or heterozygous deletion of *Adar1* in SMCs (*SMC-Adar1*$^{-/-}$: *Adar1*$^{fl/fl}$, *Myh11*^{CreERT2}, *ROSAtdTomato*, *ApoE*$^{-/-}$ or *SMC-Adar1*$^{-/+}$: *Adar1*$^{fl/WT}$, *Myh11*^{CreERT2}, *ROSAtdTomato*, *ApoE*$^{-/-}$), mice receive 2 doses of tamoxifen (200mg/kg, P.O.) at 7.5-8 weeks of age (dose 1 - day 0; and dose 2 - day 2) and started on a high fat diet as we have done previously (*39, 40*). To evaluate the effect of MDA5 KD on *Adar1* KD background, we crossed the *Ifih1*$^{-/-}$ mouse (B6.Cg-*Ifih1*$^{tm1.1Cln}$/J) that we have used previously (*52*), onto the above background in a heterozygous manner to generate SMC *Adar1*$^{-/-}$ x MDA5$^{-/+}$ mice (Adar$^{flox/flox}$, *Ifih1*$^{-/+}$, Myh11^{CreERT2}, ROSAtdT/+, ApoE$^{-/-}$) or SMC *Adar1*$^{-/-}$ x MDA5$^{-/-}$ mice (Adar$^{flox/flox}$, *Ifih1*$^{-/-}$, Myh11^{CreERT2}, ROSAtdT/+, ApoE$^{-/-}$).

Mouse aortic root/ascending aorta cell dissociation

Immediately after sacrifice, mice were perfused with phosphate buffered saline (PBS). The aortic root and ascending aorta were excised, up to the level of the brachiocephalic artery. Tissue was washed three times in PBS, placed into an enzymatic dissociation cocktail (2 U ml−1 Liberase (5401127001; Sigma–Aldrich) and 2 U ml−1 elastase (LS002279; Worthington) in Hank's Balanced Salt Solution (HBSS)) and incubated at 37 °C for 45min, and subsequently minced. The cell suspension was further dissociated with 1ml pipette 20X and single cell suspension was confirmed under microscope. Cells were then pelleted by centrifugation at 500g for 5 min. The enzyme solution was then discarded, and cells were resuspended in fresh HBSS and passed through a 35um filter into a FACS tube. To increase biological replication, a single mouse was used to obtain single-cell suspension and three mice were used in combination for each scRNA capture. 3 separate pairs of isolation were performed for control, *SMC-Adar1*$^{-/+}$ and *SMC-Adar1*$^{-/-}$ mice. Cells were FACS sorted based on tdTomato expression. tdT+ cells (considered to be of SMC lineage) and tdT− cells were then captured on separate but parallel runs of the same scRNA-Seq workflow (gating strategy and threshold identical to those published in previous work by Wirka et al (*29*)), and datasets were later combined for all subsequent analyses.

Mouse aortic root histology

IHC was performed according to standard protocol. Primary antibodies for CD68 rabbit polyclonal antibody (1:400 dilution; ab125212; Abcam) with secondary rabbit-on-rodent HRP polymer (RMR622; BioCare Medical) for CD68 evaluation. Hematoxylin and eosin (H&E) and Trichrome staining was performed using standard protocols using and H&E and Trichrome Stain Kits (Abcam, ab245880 and ab150686 respectively). The processed sections were visualized using a Leica DM5500 microscope objective magnifications, and images were obtained using Leica Application Suite X software. For quantification of atherosclerosis plaque area, sections obtained at equal distance measured from the superior margin of the coronary sinus were used for comparison to ensure equal level sections were obtained. Images with FITC autofluorescence and tdTomato with red channel representing SMC lineage traced cells were obtained. Areas

of interest were quantified using ImageJ (National Institutes of Health) software, and compared using a two-sided t-test. Lesion size was defined by the area encompassing the intimal edge of the lesion to the border of SMC-marker positive intima-media junction. Calcification was evaluated using Ferangi Blue Chromogen Kit 2 (Biocare Medical, FB813) following manufacturers protocol. For RNAscope, slides were processed and hybridized according to the manufacturer's protocol, with reagents from ACD Bio. All area quantification was performed in a genotype blinded fashion with image J using length information embedded in exported files. All biological replicates for each staining were performed simultaneously on position-matched aortic root sections to limit intra-experimental variance.

Single-cell capture and library preparation and sequencing

All single-cell capture and library preparation was performed in the Quertermous lab, sequencing was performed by Medgenome Inc (Foster City, CA). Cells were loaded into a 10x Genomics microfluidics chip and encapsulated with barcoded oligo-dT-containing gel beads using the 10x Genomics Chromium controller according to the manufacturer's instructions. Single-cell libraries were then constructed according to the manufacturer's instructions (Illumina). Libraries from individual samples were multiplexed into one lane before sequencing on an Illumina platform with targeted depth of 50,000 reads per cell for RNA or 400 million paired end reads per sequencing library.

Analysis of scRNA-Seq data

Fastq files from each experimental time point and mouse genotype were aligned to the reference genome (mm10) individually using CellRanger Software (10x Genomics). The dataset was then analyzed using the R package Seurat 30 and datasets were merged in Seurat using standard Merge function. The dataset was trimmed of cells expressing fewer than 2000 genes, and genes expressed in fewer than 50 cells. The number of genes, number of unique molecular identifiers and percentage of mitochondrial genes were examined to identify outliers. As an unusually high number of genes can result from a 'doublet' event, in which two different cell types are captured together with the same barcoded bead, cells with >9000 genes were discarded. Cells containing >7.5%

mitochondrial genes were presumed to be of poor quality and were also discarded. The gene expression values then underwent library-size normalization and normalized using established LogNormalize function in Seurat. No additional batch correction was performed. Principal component analysis was used for dimensionality reduction, followed by clustering in principal component analysis space using a graph-based clustering approach via Louvain algorithm. UMAP was then used for two-dimensional visualization of the resulting clusters. Pseudotime trajectory analysis was performed using Slingshot with available software. Analysis, visualization and quantification of gene expression and generation of gene modulescores were performed using Seurat's built-in function such as "FeaturePlot", "VlnPlot", "AddModuleScore", and "FindMarker."

For immunogenic RNA score, we generated an AddModuleScore 'score' that summates the expression of all 'immunogenic' RNA from a putative list that was generated by combining our data from experimental *in vitro* models (*23*) along with human genetic edQTL analysis (*12*).

HCASMC culture and in vitro genomic studies

Cells were cultured in smooth muscle growth medium (Lonza; catalog number: CC-3182) supplemented with human epidermal growth factor, insulin, human basic fibroblast growth factor and 5% FBS, according to the manufacturer's instructions. All HCASMC lines were used at passages 4–8. HCASMCs immortalized with hTert transgene were acquired from Dr. Clint Miller (UVA) were used for all calcification assays with HCASMCs between passages 31 and 35. siRNA knockdowns were performed using Lipofectamine RNAiMax (Life Technologies) using manufacturer's recommended protocol at 50pg siRNA / 100,000cells.

Phenotypic transition, calcification, and TGFβ assays: For phenotypic transition assays, HCASMC are cultured in 5% BSA and then subjected to serum starvation for 2 days. Following 2 days of serum starvation (0% BSA) HCASMCs develop a mature SMC phenotype, reintroduction of serum (5%) stimulates a more proliferative phenotype and RNA/protein is isolated 48hrs following reintroduction of serum. For calcification assays, HCASMCs are cultured in 1% BSA with 10mM beta-glycerophosphate and

8mM CaCl2 for 7 to 10 days. For TGFβ stimulation assays, we cultured HCASMC to confluency, treated with siRNA for 48 hours, and transitioned cells to a serum free condition for 48 hours. We then stimulated cells with TGFβ (10ng/mL) or control for 72 hours before we isolated RNA and performed quantitative PCR.

RNA isolation and Bulk RNA sequencing

RNA was isolated from disrupted HCASMC cells using standard RNeasy mini kit protocol (Qiagen). Isolated RNA underwent quality assessment, cDNA conversion, and library construction by Novogene (San Jose, CA). cDNA libraries were sequenced using Illumina Novoseq 6000 achieving 20-30 million paired-end reads per sample. RNAseq data were processed using a workflow starting from fastq files and code is available on github (https://github.com/zhaoshuoxp/Pipelines-Wrappers/blob/master/RNAseq.sh). In brief, the quality control was performed using FastQC, mapping to the human genome hg19/GRCh37 was performed using STAR second pass mapping to increase the percentage of mapped reads, and counting was done with featureCounts using GENCODE gtf annotation. Next, differential analysis was performed using DESeq2.

RNA editing analysis

RNA editing analysis in bulk RNA seq data was performed following a pipeline as we have done previously (*12*). Briefly, we compiled a list of reference editing sites for quantification. By incorporating known sites in the RADAR database (*53*), tissue-specific sites identified in GTEx V6p17, and recently published hyper-editing sites (*54*), we finalized a list of 2,802,572 human editing sites. To quantify the editing levels, we computed the ratio of G reads divided by the sum of A and G reads at each site. Because the bulk RNA-seq data from HCASMC cells was not strand specific, the reads cannot be automatically assigned to sense and antisense strands, so that the quantification of editing level may be affected by expression of either of the two overlapping genes. Therefore, we developed a method to measure the RNA editing level of a given site using the reads derived from the corresponding transcript (sense for A-to-G edits and antisense for T-to-C edits), with less influence by the other overlapping transcript. For reads that are edited, they would be derived from the sense transcript if

the edits are A-to-G, and from the antisense transcript if the edits are T-to-C. For the rest of the reads that are unedited, we estimated the numbers derived from the sense versus antisense transcripts in proportion to their expression levels. Overall RNA editing frequency was reported as percentage of total RNA editing sites across the genome.

List of Supplementary Materials

- Supplemental Figure 1. *Loss of ADAR1 in human coronary artery SMCs (HCASMCs) regulates viral sensing transcriptomic response in vitro*.
- Supplemental Figure 2. Global RNA editing is decreased in HCASMC following phenotypic modulation in vitro
- Supplemental Figure 3. *Serum and TGFβ stimulation upregulate ADAR1 expression with differential effect on ISG induction in HCASMC.*
- Supplemental Figure 4. *Loss of ADAR1 regulates transcriptomic and inflammatory response to calcification in vitro*.
- Supplemental Figure 5. Quantification of histological findings for (A) loss of elastin organization, (B) adventitial ballooning, and (C) intramural hemorrhage.
- Supplemental Figure 6. *SMC Adar1 KD induces antiviral defense transcriptional pathways.*
- Supplemental Figure 7. *Loss of SMC Adar1 coordinates distinct response throughout vessel wall.*
- Supplemental Figure 8. SMC Adar1 het versus control following 16 weeks high fat diet in atherosclerosis model for (A) weight, (B) LDL cholesterol, (C) triglycerides, (D) total cholesterol, (E) HDL cholesterol.
- Supplemental Figure 9. *SMC specific haploinsufficiency of Adar1 in SMC subset analysis shows ISG activation with phenotypic modulation in atherosclerosis.*
- Supplemental Figure 10. *SMC specific haploinsufficiency of Adar1 increases vascular chondromyoctye formation*
- Supplemental Figure 11. ISG dependent trajectory analysis from SMC to CMC implicates distinct gene ontologies.

- Supplemental Figure 12. *Isg15 RNAscope reveals increased Isg15 signal in plaque of SMC Adar1$^{-/+}$ mice.*
- Supplemental Figure 13. SMC specific haploinsufficiency in Adar1 increased SMC lineage traced cell content in plaque without change in acellular area.

References

1. G. B. D. Diseases, C. Injuries, Global burden of 369 diseases and injuries in 204 countries and territories, 1990-2019: a systematic analysis for the Global Burden of Disease Study 2019. *Lancet* **396**, 1204-1222 (2020).
2. M. Nikpay *et al.*, A comprehensive 1,000 Genomes-based genome-wide association meta-analysis of coronary artery disease. *Nat Genet* **47**, 1121-1130 (2015).
3. H. Schunkert *et al.*, Large-scale association analysis identifies 13 new susceptibility loci for coronary artery disease. *Nat Genet* **43**, 333-338 (2011).
4. P. van der Harst, N. Verweij, Identification of 64 Novel Genetic Loci Provides an Expanded View on the Genetic Architecture of Coronary Artery Disease. *Circ Res* **122**, 433-443 (2018).
5. C. Tcheandjieu *et al.*, Large-scale genome-wide association study of coronary artery disease in genetically diverse populations. *Nat Med* **28**, 1679-1692 (2022).
6. F. W. Albert, L. Kruglyak, The role of regulatory variation in complex traits and disease. *Nat Rev Genet* **16**, 197-212 (2015).
7. G. T. Consortium, The GTEx Consortium atlas of genetic regulatory effects across human tissues. *Science* **369**, 1318-1330 (2020).
8. E. Eisenberg, E. Y. Levanon, A-to-I RNA editing - immune protector and transcriptome diversifier. *Nat Rev Genet* **19**, 473-490 (2018).
9. N. Jonkhout *et al.*, The RNA modification landscape in human disease. *RNA* **23**, 1754-1769 (2017).
10. C. R. Walkley, J. B. Li, Rewriting the transcriptome: adenosine-to-inosine RNA editing by ADARs. *Genome Biol* **18**, 205 (2017).
11. A. Gatsiou, K. Stellos, RNA modifications in cardiovascular health and disease. *Nat Rev Cardiol* **20**, 325-346 (2023).
12. Q. Li *et al.*, RNA editing underlies genetic risk of common inflammatory diseases. *Nature* **608**, 569-577 (2022).

13. H. Chung *et al.*, Human ADAR1 Prevents Endogenous RNA from Triggering Translational Shutdown. *Cell* **172**, 811-824 e814 (2018).
14. B. J. Liddicoat *et al.*, RNA editing by ADAR1 prevents MDA5 sensing of endogenous dsRNA as nonself. *Science* **349**, 1115-1120 (2015).
15. D. Goubau, S. Deddouche, C. Reis e Sousa, Cytosolic sensing of viruses. *Immunity* **38**, 855-869 (2013).
16. A. M. Chalk, S. Taylor, J. E. Heraud-Farlow, C. R. Walkley, The majority of A-to-I RNA editing is not required for mammalian homeostasis. *Genome Biol* **20**, 268 (2019).
17. K. Nishikura, Functions and regulation of RNA editing by ADAR deaminases. *Annual review of biochemistry* **79**, 321-349 (2010).
18. K. Pestal *et al.*, Isoforms of RNA-Editing Enzyme ADAR1 Independently Control Nucleic Acid Sensor MDA5-Driven Autoimmunity and Multi-organ Development. *Immunity* **43**, 933-944 (2015).
19. N. M. Mannion *et al.*, The RNA-editing enzyme ADAR1 controls innate immune responses to RNA. *Cell reports* **9**, 1482-1494 (2014).
20. A. Feigenbaum *et al.*, Singleton-Merten syndrome: an autosomal dominant disorder with variable expression. *Am J Med Genet A* **161A**, 360-370 (2013).
21. F. Rutsch, I. Buers, Y. Nitschke, Hereditary Disorders of Cardiovascular Calcification. *Arterioscler Thromb Vasc Biol* **41**, 35-47 (2021).
22. C. A. Emdin *et al.*, Analysis of predicted loss-of-function variants in UK Biobank identifies variants protective for disease. *Nat Commun* **9**, 1613 (2018).
23. T. Sun *et al.*, A Small Subset of Cytosolic dsRNAs Must Be Edited by ADAR1 to Evade MDA5-Mediated Autoimmunity. *bioRxiv*, 2022.2008.2029.505707 (2022).
24. T. Alsaigh, D. Evans, D. Frankel, A. Torkamani, Decoding the transcriptome of calcified atherosclerotic plaque at single-cell resolution. *Commun Biol* **5**, 1084 (2022).
25. M. R. Alexander, G. K. Owens, Epigenetic control of smooth muscle cell differentiation and phenotypic switching in vascular development and disease. *Annu Rev Physiol* **74**, 13-40 (2012).

26. G. L. Basatemur, H. F. Jorgensen, M. C. H. Clarke, M. R. Bennett, Z. Mallat, Vascular smooth muscle cells in atherosclerosis. *Nat Rev Cardiol* **16**, 727-744 (2019).
27. P. Cheng *et al.*, ZEB2 Shapes the Epigenetic Landscape of Atherosclerosis. *Circulation*, (2022).
28. J. B. Kim *et al.*, Environment-Sensing Aryl Hydrocarbon Receptor Inhibits the Chondrogenic Fate of Modulated Smooth Muscle Cells in Atherosclerotic Lesions. *Circulation* **142**, 575-590 (2020).
29. R. C. Wirka *et al.*, Atheroprotective roles of smooth muscle cell phenotypic modulation and the TCF21 disease gene as revealed by single-cell analysis. *Nat Med* **25**, 1280-1289 (2019).
30. P. Cheng *et al.*, Smad3 regulates smooth muscle cell fate and mediates adverse remodeling and calcification of the atherosclerotic plaque. *Nature Cardiovascular Research* **1**, 322-333 (2022).
31. H. J. Kim *et al.*, Molecular mechanisms of coronary artery disease risk at the PDGFD locus. *Nat Commun* **14**, 847 (2023).
32. D. Sharma *et al.*, Comprehensive Integration of Multiple Single-Cell Transcriptomic Data Sets Defines Distinct Cell Populations and Their Phenotypic Changes in Murine Atherosclerosis. *Arterioscler Thromb Vasc Biol* **44**, 391-408 (2024).
33. G. Ramaswami *et al.*, Accurate identification of human Alu and non-Alu RNA editing sites. *Nat Methods* **9**, 579-581 (2012).
34. L. S. Shankman *et al.*, KLF4-dependent phenotypic modulation of smooth muscle cells has a key role in atherosclerotic plaque pathogenesis. *Nat Med* **21**, 628-637 (2015).
35. M. Maurano *et al.*, Protein kinase R and the integrated stress response drive immunopathology caused by mutations in the RNA deaminase ADAR1. *Immunity* **54**, 1948-1960 e1945 (2021).
36. D. Wong *et al.*, FHL5 Controls Vascular Disease-Associated Gene Programs in Smooth Muscle Cells. *Circ Res* **132**, 1144-1161 (2023).

37. D. Cai *et al.*, A Novel Mechanism Underlying Inflammatory Smooth Muscle Phenotype in Abdominal Aortic Aneurysm. *Circ Res* **129**, e202-e214 (2021).
38. J. Fei, X. B. Cui, J. N. Wang, K. Dong, S. Y. Chen, ADAR1-Mediated RNA Editing, A Novel Mechanism Controlling Phenotypic Modulation of Vascular Smooth Muscle Cells. *Circ Res* **119**, 463-469 (2016).
39. P. Cheng *et al.*, Smad3 regulates smooth muscle cell fate and mediates adverse remodeling and calcification of the atherosclerotic plaque. *Nat Cardiovasc Res* **1**, 322-333 (2022).
40. P. Cheng *et al.*, ZEB2 Shapes the Epigenetic Landscape of Atherosclerosis. *Circulation* **145**, 469-485 (2022).
41. U. Lendahl, L. Muhl, C. Betsholtz, Identification, discrimination and heterogeneity of fibroblasts. *Nat Commun* **13**, 3409 (2022).
42. S. Jin *et al.*, Inference and analysis of cell-cell communication using CellChat. *Nat Commun* **12**, 1088 (2021).
43. J. W. Tyner *et al.*, CCL5-CCR5 interaction provides antiapoptotic signals for macrophage survival during viral infection. *Nat Med* **11**, 1180-1187 (2005).
44. K. Street *et al.*, Slingshot: cell lineage and pseudotime inference for single-cell transcriptomics. *BMC Genomics* **19**, 477 (2018).
45. R. M. Plenge, E. M. Scolnick, D. Altshuler, Validating therapeutic targets through human genetics. *Nat Rev Drug Discov* **12**, 581-594 (2013).
46. E. Mountjoy *et al.*, An open approach to systematically prioritize causal variants and genes at all published human GWAS trait-associated loci. *Nat Genet* **53**, 1527-1533 (2021).
47. K. Estrada *et al.*, Identifying therapeutic drug targets using bidirectional effect genes. *Nat Commun* **12**, 2224 (2021).
48. T. Roychowdhury *et al.*, Genome-wide association meta-analysis identifies risk loci for abdominal aortic aneurysm and highlights PCSK9 as a therapeutic target. *Nat Genet* **55**, 1831-1842 (2023).
49. O. Soehnlein, P. Libby, Targeting inflammation in atherosclerosis - from experimental insights to the clinic. *Nat Rev Drug Discov* **20**, 589-610 (2021).

50. P. M. Ridker *et al.*, Antiinflammatory Therapy with Canakinumab for Atherosclerotic Disease. *N Engl J Med* **377**, 1119-1131 (2017).
51. J. W. Schoggins, Interferon-Stimulated Genes: What Do They All Do? *Annu Rev Virol* **6**, 567-584 (2019).
52. S. B. Hu *et al.*, ADAR1p150 prevents MDA5 and PKR activation via distinct mechanisms to avert fatal autoinflammation. *Mol Cell* **83**, 3869-3884 e3867 (2023).
53. G. Ramaswami, J. B. Li, RADAR: a rigorously annotated database of A-to-I RNA editing. *Nucleic Acids Res* **42**, D109-113 (2014).
54. H. T. Porath, B. A. Knisbacher, E. Eisenberg, E. Y. Levanon, Massive A-to-I RNA editing is common across the Metazoa and correlates with dsRNA abundance. *Genome Biol* **18**, 185 (2017).

Acknowledgements

Funding:

National Institutes of Health grant F32HL160067 (CW)
National Institutes of Health grant L30HL159413 (CW)
National Institutes of Health grant K08HL167699 (CW)
National Institutes of Health grant K08HL153798 (PC)
National Institutes of Health grant R01HL134817 (TQ)
National Institutes of Health grant R01HL139478 (TQ)
National Institutes of Health grant R01HL156846 (TQ)
National Institutes of Health grant R01HL151535 (TQ)
National Institutes of Health grant R01HL145708 (TQ)
National Institutes of Health grant UM1 HG011972 (TQ)
National Institutes of Health grant R35GM144100 (JBL)
National Institutes of Health grant R01MH115080 (JBL)
National Institutes of Health grant R01GM102484 (JBL)
American Heart Association grant 20CDA35310303 (PC)
American Heart Association grant 23CDA1042900 (CW)
American Heart Association grant 23POST1018991 (WG).

Author Contributions

Conceptualization: C.W., Q.L., P.C., J.B.L., and T.Q.

Methodology: C.W., Q.L., J.M.

Investigation: C.W., Q.L., J.M., H.G., D.G., W.G., M.W., Q.Z., M.R., D.L., B.P., A.B., R.K., T.N.
Visualization: C.W.
Funding acquisition: C.W., J.B.L., T.Q.
Project administration: C.W., J.B.L., T.Q.
Supervision: J.B.L., T.Q.
Writing — original draft: C.W., J.B.L., T.Q.
Writing — review and editing: C.W., Q.L., J.B.L., T.Q.

Competing interests:

C.W. is a consultant for AiRNA Bio and Avidity Biosciences. T.Q. serves on the scientific advisory board for Amgen. J.B.L. is a co-founder of AIRNA Bio and a consultant for Risen Pharma. J.B.L. and Q.L. are named inventors of a provisional patent filed by Stanford University (serial no. 63/473,678), describing a method related to RNA editing. The other authors declare no competing interests.

Data and materials availability:

All raw and processed sequencing data are deposited in the National Center for Biotechnology Information Gene Expression Omnibus. Bulk and single cell RNA sequencing data is available through accession IDs GSE254862 and GSE255661 respectively.

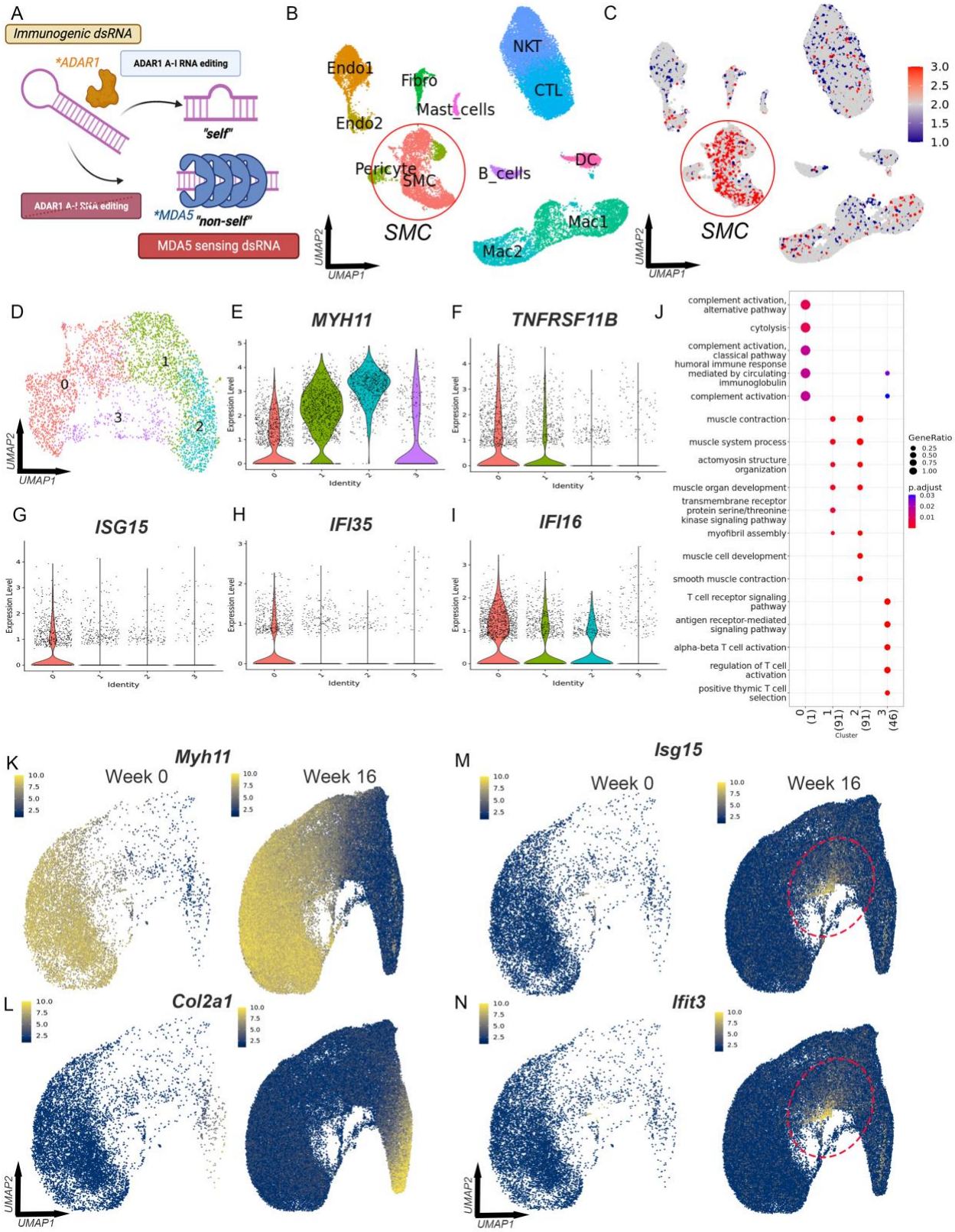

Figure 1. ***Smooth muscle cells in atherosclerosis express immunogenic RNA and show evidence of ISG induction in phenotypic modulation.*** (A) Schematic of

ADAR1 RNA editing of dsRNA. (B) UMAP of scRNAseq data from human carotid atherosclerotic plaque (Alsaigh et al., 2022). (C) Module score of immunogenic RNA expression. (D) Clustering of SMC subset with (E) violin plot showing SMC marker *MYH11* with (F) fibromyocyte/chondromyocyte marker *TNFRSF11B*. (G-I) Violin plots of ISGs *ISG15* (G), *IF135* (H), and *IFI16* (I). (J) GO-term enrichment analysis for human athero SMC clustering. (K-N) In mouse comprehensive integrated dataset of lineage traced SMCs (from Sharma et al., 2024), featureplot of *Myh11* (K) and *Col2a1* (L) at 0 and 16 weeks of high fat diet. (L-M) Featureplots of *Isg15* (L) and *Ifit3* (M) in SMC phenotypic modulation.

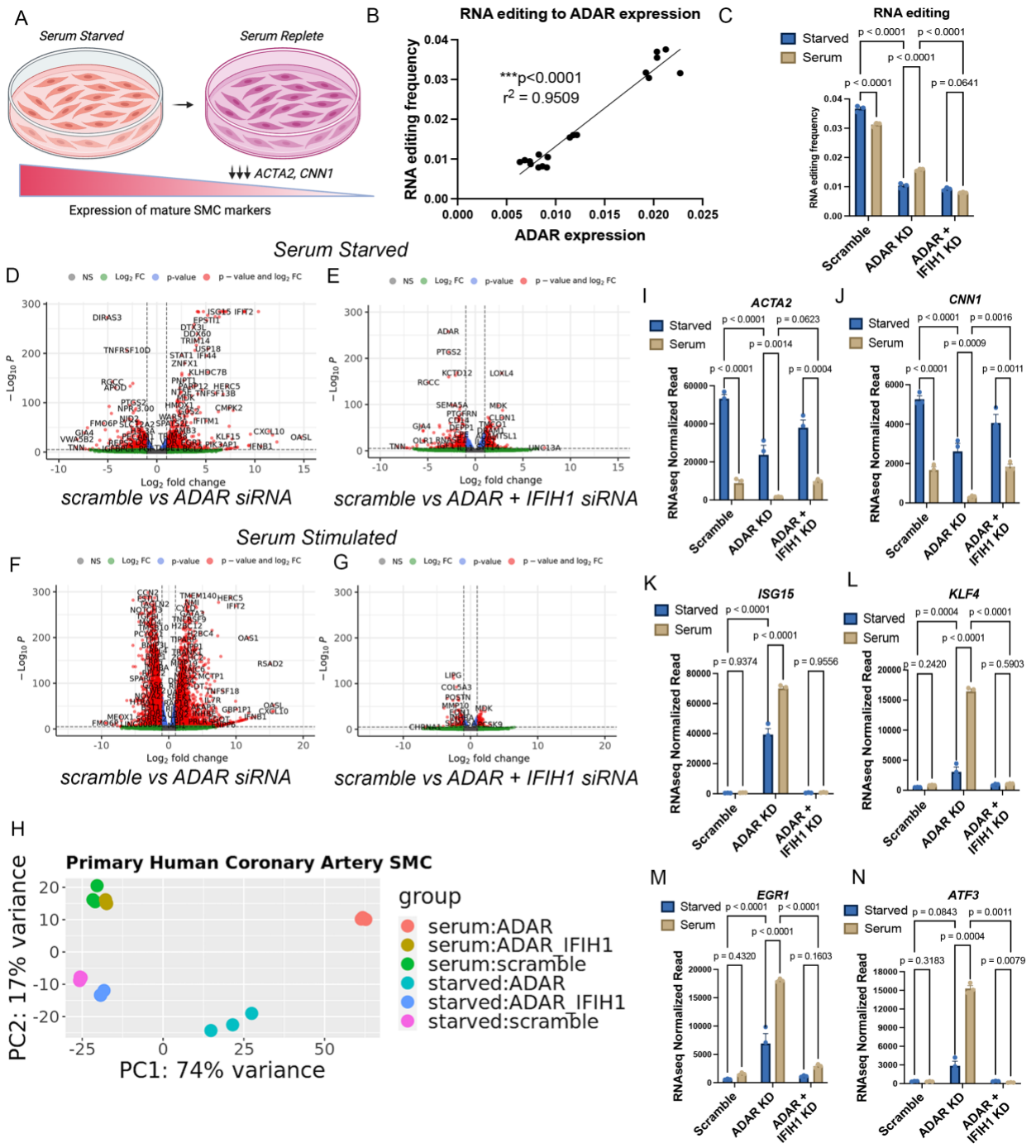

Figure 2. ***ADAR1 regulates RNA editing in human coronary SMCs and RNA editing requirement is dependent on cell context.*** (A) Schematic of SMC phenotypic modulation in vitro assay. (B) Linear regression analysis of ADAR1 expression and global RNA editing frequency in primary human coronary artery SMCs (HCASMCs) following siRNA KD of *ADAR*. (C) Grouped bar chart of RNA editing frequency with cellular treatment of scramble, *ADAR*, and *ADAR* + *IFIH1* (MDA5) siRNA. (D) Volcano

plot of bulk RNAseq DE gene analysis comparing scramble vs *ADAR* siRNA in serum starved conditions, (E) volcano plot comparing scramble vs *ADAR* + *IFIH1* siRNA in serum starved conditions, (F) volcano plot comparing scramble vs *ADAR* siRNA in serum fed conditions, and (G) volcano plot comparing scramble vs *ADAR* + *IFIH1* siRNA in serum fed conditions. (H) Principal component analysis (PCA) of bulk RNAseq data of principal components 1 and 2 for each HCASMC treatment. Grouped bar chart of normalized RNAseq reads across HCASMC treatments for (I) *ACTA2*, (J) *CNN1*, (K) *ISG15*, (L) *KLF4*, (M) *EGR1*, and (N) *ATF3*. *P*-values represent simple linear regression (B) or (C, I-N) two-way ANOVA with multiple comparisons post hoc analysis. N = 3 RNA seq libraries per condition.

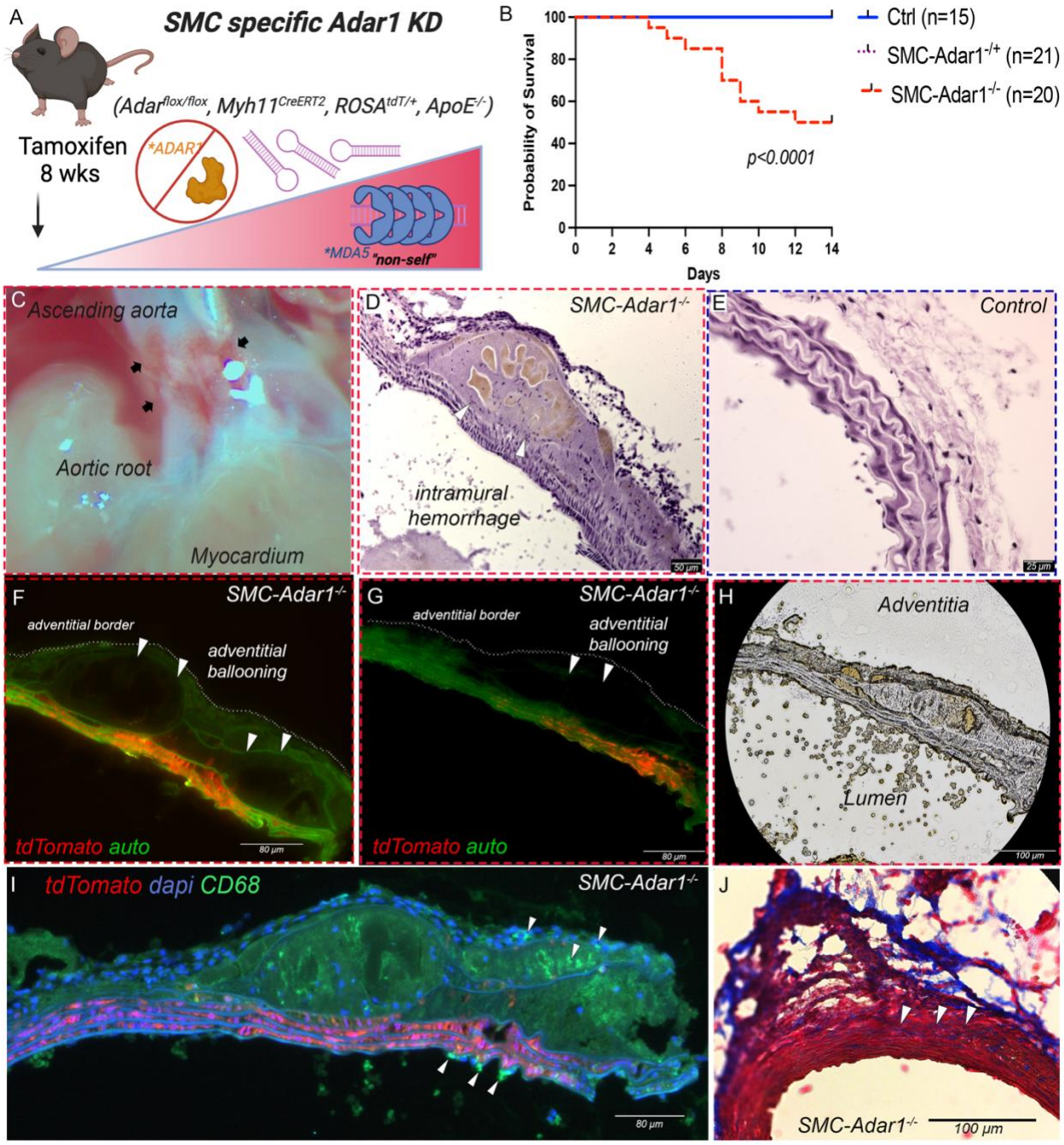

Figure 3*. SMC specific ADAR1 is required to maintain vascular integrity and survival.* (A) Schematic of SMC-*Adar1*$^{-/-}$ model and accumulation of dsRNA and MDA5 activation. (B) Survival curves for 56 mice treated with tamoxifen at 8 weeks of age, comparing *SMC-Adar1*$^{-/-}$, *SMC-Adar1*$^{-/+}$ (*Adar1*$^{fl/WT}$, *Myh11*^{CreERT2}, *ROSAtdTomato*, *ApoE*$^{-/-}$), and control (*Adar1*$^{WT/WT}$, *Myh11*^{CreERT2}, *ROSAtdTomato*, *ApoE*$^{-/-}$) genotypes. (C) Gross image of aortic root and ascending aorta of *SMC-Adar1*^{KO} mouse at 2 weeks

following tamoxifen treatment. (D-E) Representative images of hematoxylin and eosin (H&E) staining from *SMC-Adar1*$^{-/-}$ (D) and control genotype mice (E). (F-G) Fluorescent imaging with autofluorescence indicating elastin (green) and Myh11 derived cells labeled with tdTomato (red) in two mice with adventitial ballooning in *SMC-Adar1*$^{-/-}$ (F-G). (H) Bright field imaging of aorta cross section from *SMC-Adar1*$^{-/-}$ mouse corresponding to fluorescent imaging in panel G. (I) Cd68 immunostaining of aorta cross section from *SMC-Adar1*$^{-/-}$ mouse showing macrophage infiltration. (J) Masson trichrome stain of aorta cross section from *SMC-Adar1*$^{-/-}$ mouse showing intra-medial collagen deposition. *P*-value represents comparison of survival curves, Log-rank (Mantel-Cox) test (B).

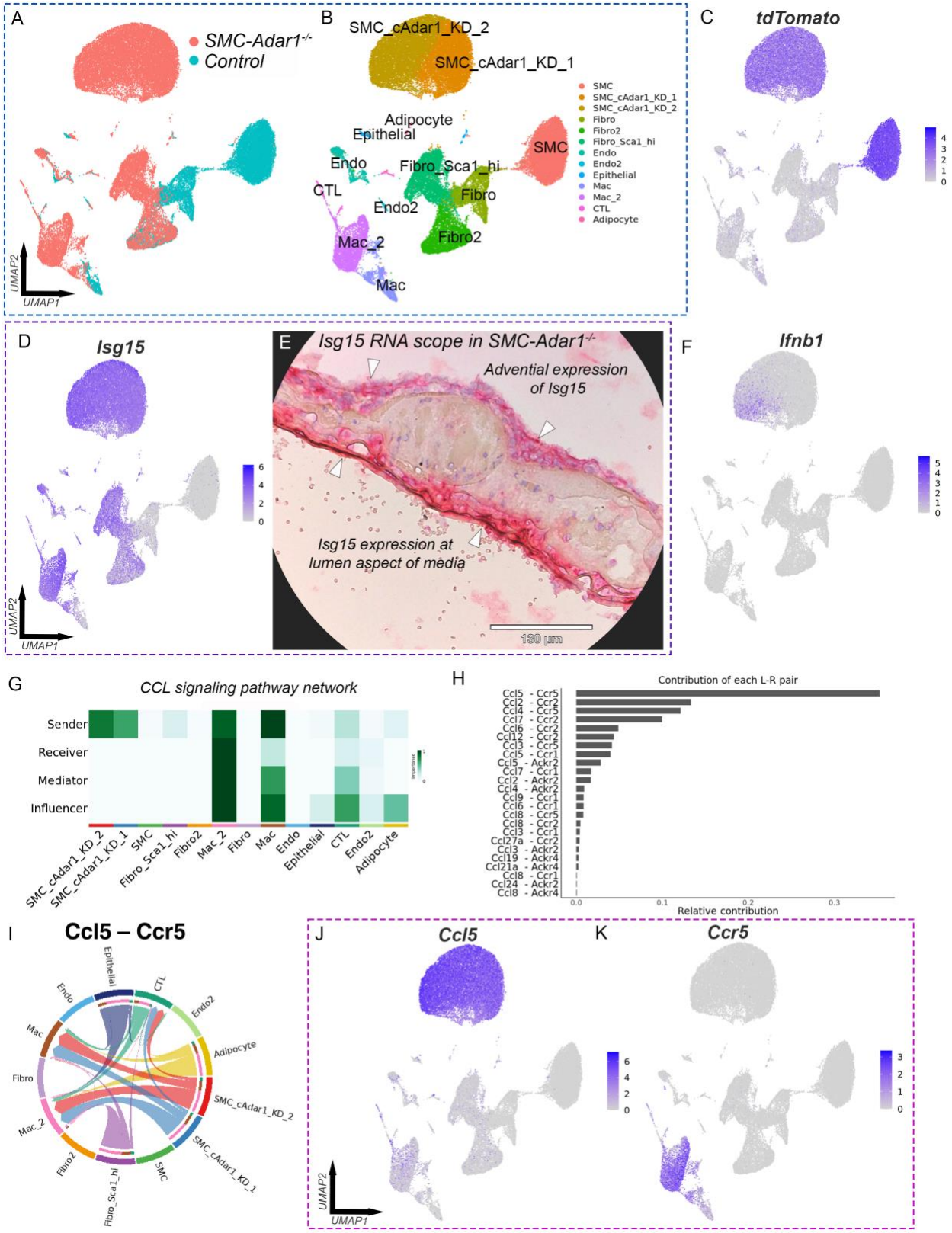

Figure 4. ***Single cell RNA sequencing reveals SMC Adar1 to control ISG activation, phenotypic response, and macrophage infiltration*****.** (A) scRNAseq

UMAP from aortic root and ascending aorta grouped by genotype of *SMC-Adar1*$^{-/-}$ (*Adar1*$^{fl/fl}$, *Myh11*^{CreERT2}, *ROSAtdTomato*, *ApoE*$^{-/-}$) and control (*Adar1*$^{WT/WT}$, *Myh11*^{CreERT2}, *ROSAtdTomato*, *ApoE*$^{-/-}$) genotypes at 2 weeks following tamoxifen treatment. (B) UMAP with clustering and cell type identification of combined *SMC-Adar1*$^{-/-}$ and control genotype data. (C) Featureplot of tdTomato showing SMC lineage tracing. (D) Featureplot of *Isg15*. (E) RNAscope of *Isg15* in aortic tissue of *SMC-Adar1*$^{-/-}$ mice showing highest *Isg15* expression at the lumen aspect of media, with additional adventitial expression. (F) Featureplot of *Ifnb1*. (G) Heatmap of network centrality scores for CCL signaling network across cell clusters. (H) Contributions of each receptor-ligand pair for CCL signaling. (I) Chord diagram of receptor-ligand interaction between clusters for CCL5:CCR5. (J-K) Featureplot of (J) *Ccl5* and (K) *Ccr5*.

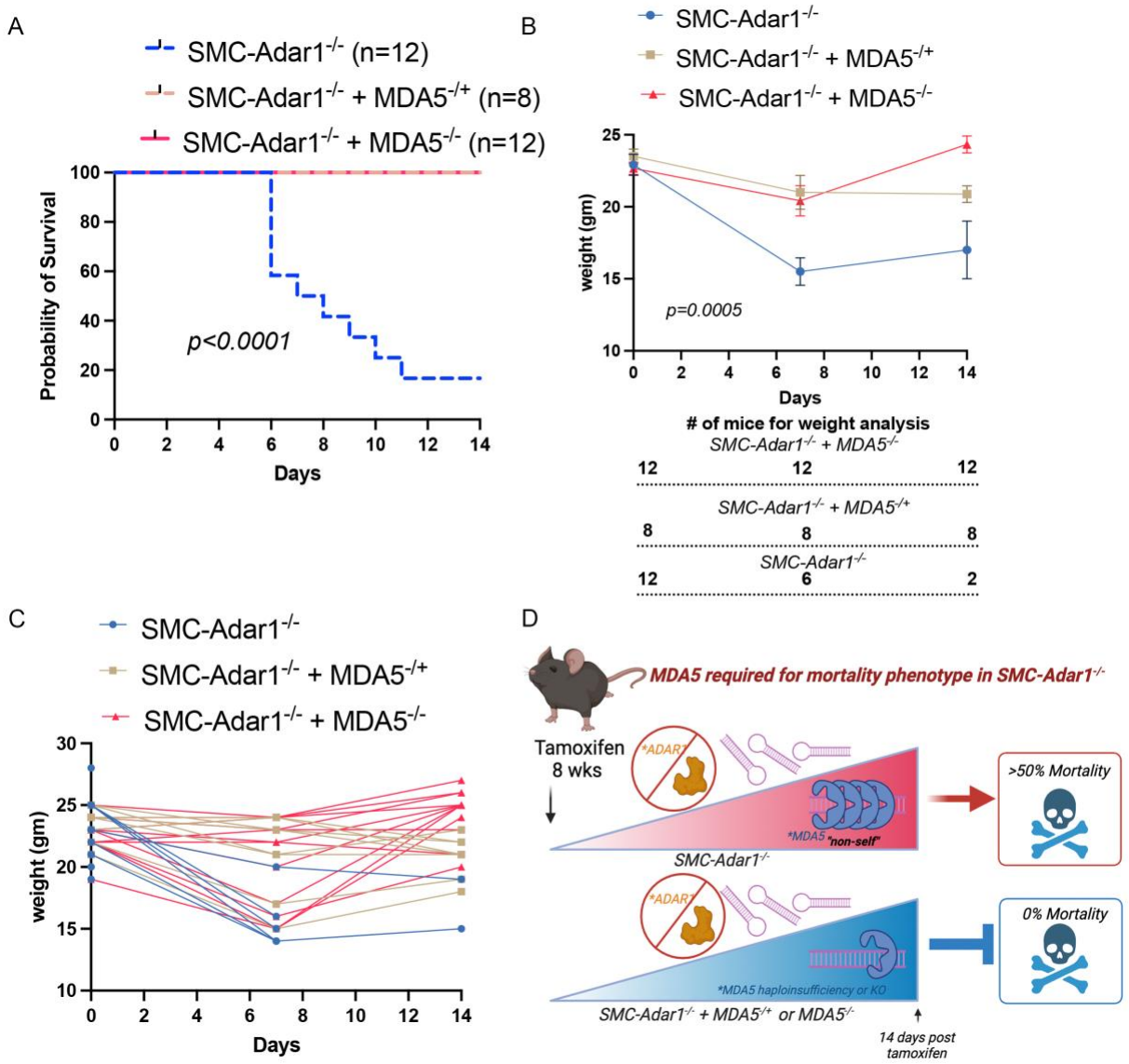

Figure 5. ***Haploinsufficiency in MDA5 is adequate to prevent mortality in SMC-Adar1$^{-/-}$ mice.*** (A) Survival curves for *SMC-Adar1$^{-/-}$* (*Adar1$^{fl/fl}$*, *Myh11^{CreERT2}*, *ROSAtdTomato*, *ApoE$^{-/-}$*), *SMC-Adar1$^{-/-}$ + MDA5$^{-/+}$* (*Adar1$^{fl/fl}$*, *Ifih1$^{-/+}$*, *Myh11^{CreERT2}*, *ROSAtdTomato*, *ApoE$^{-/-}$*), and *SMC-Adar1$^{-/-}$ + MDA5$^{-/-}$* (*Adar1$^{fl/fl}$*, *Ifih1$^{-/-}$*, *Myh11^{CreERT2}*, *ROSAtdTomato*, *ApoE$^{-/-}$*) genotypes following tamoxifen treatment at 8 weeks of age. (B) Weight curve at 0, 7, and 14 days following tamoxifen treatment between genotypes of surviving mice. (C) Individual weight measures at 0, 7, and 14 days following tamoxifen treatment between genotypes of surviving mice. (D) Schematic diagram of *SMC-Adar1$^{-/-}$* and MDA5 haploinsufficiency or global KO protecting against mortality. *P-*

values represent comparison of survival curves Log-rank (Mantel-Cox) test (A-B). (B) Data point represents means (±SEM).

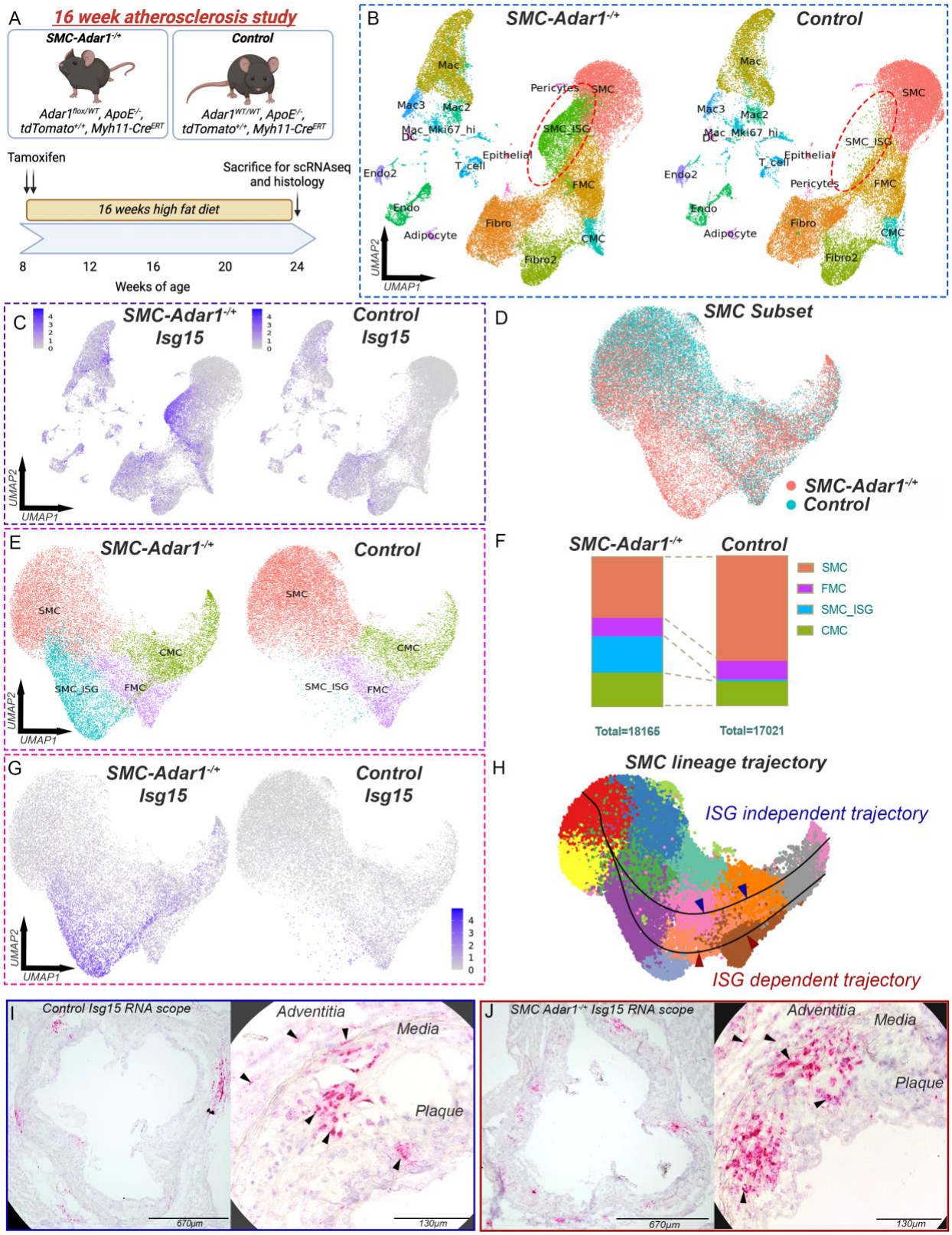

Figure 6. ***SMC specific haploinsufficiency of Adar1 activates the ISG response in atherosclerosis increasing vascular chondromyoctye formation.*** (A) UMAP of

scRNAseq data from atherosclerotic aortic root and ascending aorta at 16 weeks high fat diet split by *SMC-Adar1*$^{-/+}$ (*Adar1*$^{fl/WT}$, *Myh11*^{CreERT2}, *ROSAtdTomato*, *ApoE*$^{-/-}$) and control (*Adar1*$^{WT/WT}$, *Myh11*^{CreERT2}, *ROSAtdTomato*, *ApoE*$^{-/-}$) genotypes. (B) UMAP of grouped *SMC-Adar1*$^{-/+}$ and control genotypes. (C) Featureplot of *Isg15* split by genotype. (D) UMAP of SMC subset analysis grouped by genotype. (E) UMAP of SMC subset cluster analysis split by genotype showing SMC, SMC_ISG (interferon stimulated gene), fibromyocyte (FMC), and chondromyocyte (CMC) cell clusters. (F) Stacked bar chart showing cell populations of SMC subset for SMC, SMC_ISG, FMC, and CMC clusters. (G) Featureplot of *Isg15* in SMC subset split by genotype. (H) Lineage trajectory analysis using slingshot within SMC subset showing two distinct lineages (SMC_ISG dependent and independent) from SMC to CMC. (I&J) RNA scope for *Isg15* in aortic root sections in control (I) and *SMC-Adar1*$^{-/+}$ (J) mice.

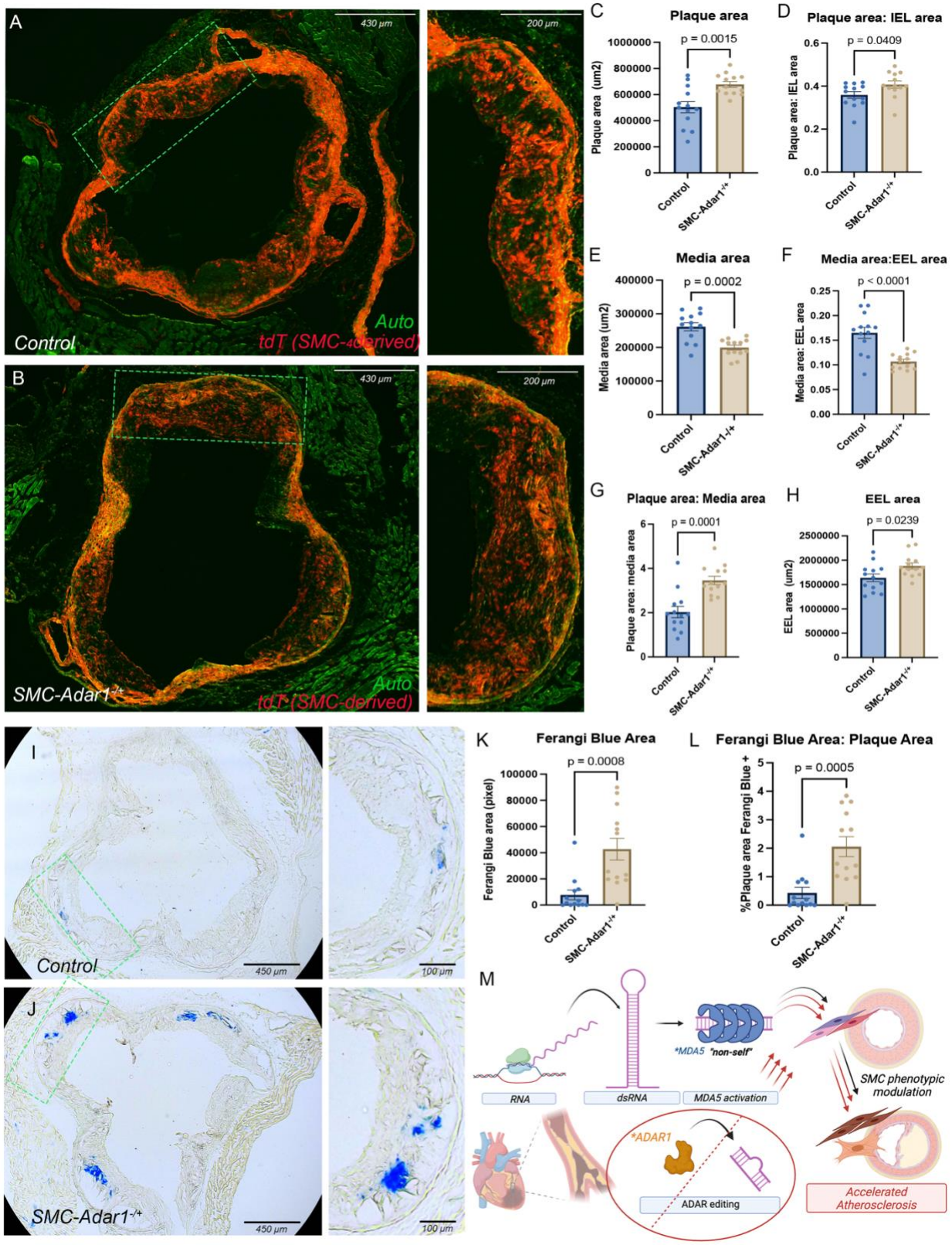
A
430 µm
200 µm
Control
Auto
tdT (SMC-derived)
B
SMC-Adar1-/+
C
Plaque area
p = 0.0015
Plaque area (um2)
Control
SMC-Adar1-/+
D
Plaque area: IEL area
p = 0.0409
Plaque area: IEL area
E
Media area
p = 0.0002
Media area (um2)
F
Media area:EEL area
p < 0.0001
Media area: EEL area
G
Plaque area: Media area
p = 0.0001
Plaque area: media area
H
EEL area
p = 0.0239
EEL area (um2)
I
450 µm
100 µm
J
K
Ferangi Blue Area
p = 0.0008
Ferangi Blue area (pixel)
L
Ferangi Blue Area: Plaque Area
p = 0.0005
%Plaque area Ferangi Blue +
M
RNA
dsRNA
MDA5 activation
*MDA5
"non-self"
SMC phenotypic modulation
*ADAR1
ADAR editing
Accelerated Atherosclerosis

Figure 7. ***SMC specific haploinsufficiency in Adar1 increases plaque size and calcification in atherosclerosis.*** Representative fluorescent images of aortic root plaque histology in *SMC-Adar1*$^{-/+}$ and control genotypes (A&B) with quantification of plaque area (C), plaque area normalized to internal elastic lamina area (IEL) (D), media area (E), media area normalized to external elastic lamina area (EEL) (F), plaque area normalized to media area (G), and EEL area (H). Representative images of Ferangi Blue calcification staining in *SMC-Adar1*$^{-/+}$ and control genotypes (I&J), quantification of Ferangi Blue area (K), and Ferangi Blue area normalized to plaque area (L). (M) Schematic diagram showing mechanism of dsRNA formation, MDA5 activation, and impaired RNA editing by ADAR1 to accelerate SMC phenotypic modulation, calcification, and atherosclerosis. Data represent mean +/- SEM, N = 13 per group. *P*-values represent unpaired two-tailed T-test.

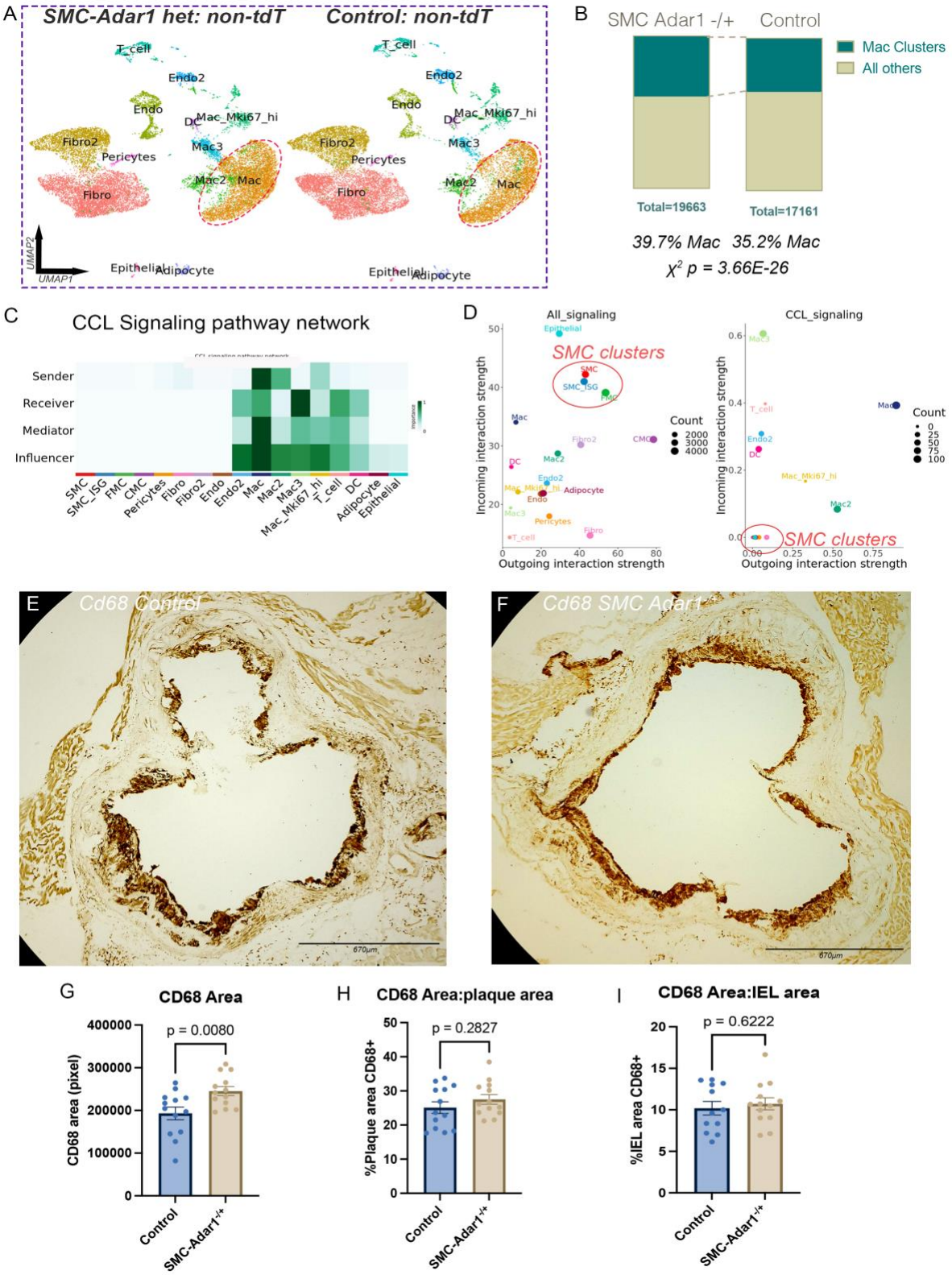

Figure 8. ***SMC specific haploinsufficiency of Adar1 has minimal effect on macrophage infiltration in atherosclerosis.*** (A) UMAP of scRNAseq data of non-

tdTomato lineage traced cells from atherosclerotic aortic root and ascending aorta at 16 weeks high fat diet split by *SMC-Adar1*$^{-/+}$ and control genotypes. (B) Stacked bar chart comparing proportion of macrophage cell population between *SMC-Adar1*$^{-/+}$ and control genotypes. (C) Heatmap of network centrality scores for CCL signaling network across cell clusters. (D) Dot plot of outgoing and incoming interaction strength across cell clusters for all signaling networks (left) and CCL signaling network (right). (E-F) Cd68 immunohistochemical staining within the aortic root following in control (E) and *SMC-SMC-Adar1*$^{-/+}$ (F) mice. (G) Total area of Cd68 positive stain showing a significant increase in Cd68 in *SMC-Adar1*$^{-/+}$ compared to control, however this effect is not significant when normalizing to (H) plaque area, or (I) vessel area at the internal elastic lamina (IEL). *P*-values represent chi-squared test (B) and unpaired two-tailed T-test (G-I).